UNIVERSIDADE FEDERAL DO PARANÁ

ORIDES WLADISLAU GOLYJESWSKI

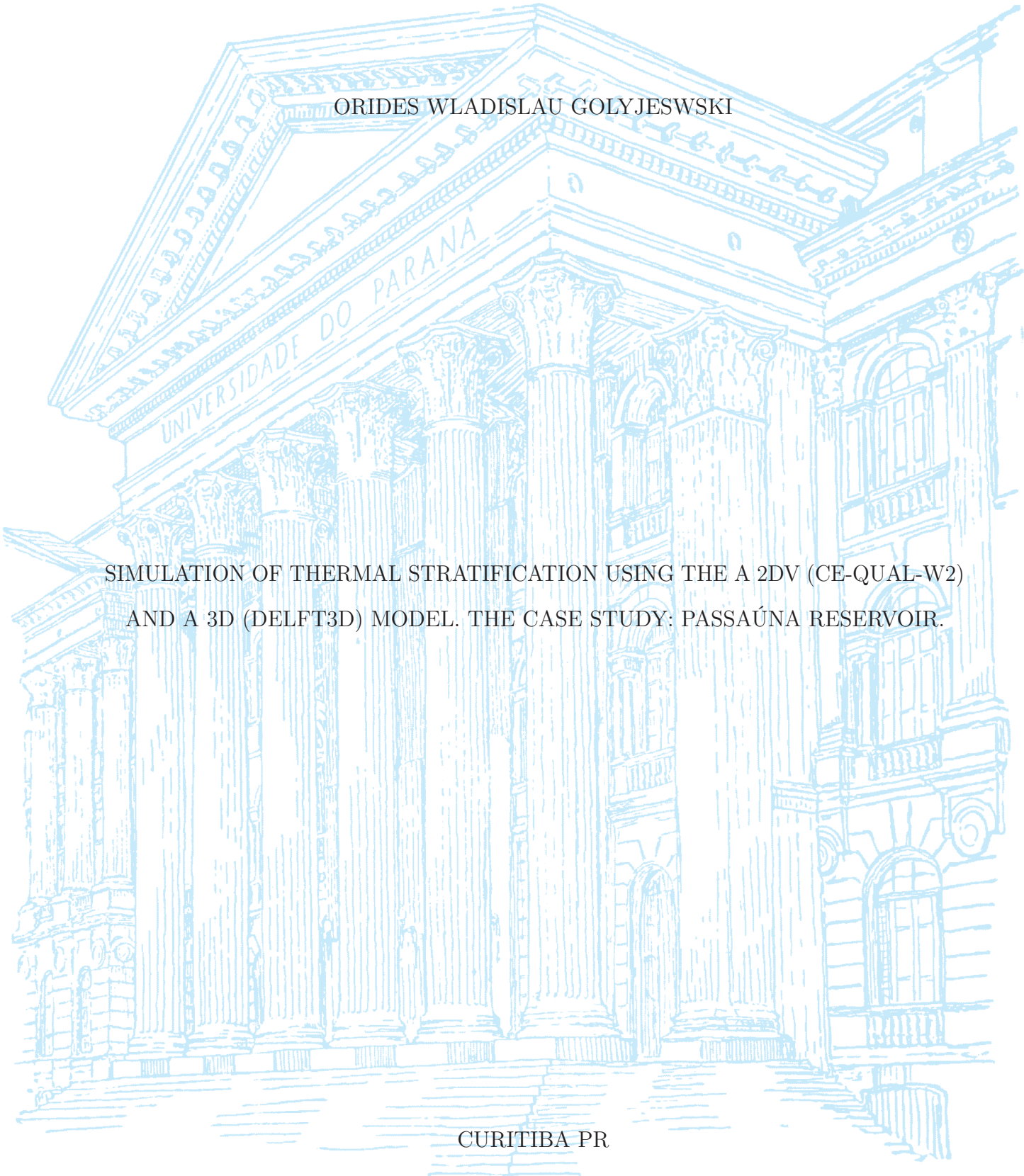


# SIMULATION OF THERMAL STRATIFICATION USING THE A 2DV (CE-QUAL-W2) AND A 3D (DELFT3D) MODEL. THE CASE STUDY: PASSAÚNA RESERVOIR.

CURITIBA PR

2020

ORIDES WLADISLAU GOLYJESWSKI

# SIMULATION OF THERMAL STRATIFICATION USING THE A 2DV (CE-QUAL-W2) AND A 3D (DELFT3D) MODEL. THE CASE STUDY: PASSAÚNA RESERVOIR.

Dissertação apresentada como requisito parcial à obtenção do grau de Mestre em Engenharia Ambiental no Programa de Pós-Graduação em Engenharia Ambiental, Setor de Tecnologia, da Universidade Federal do Paraná.

Advisor: Tobias B. Bleninger.

CURITIBA PR

2020

Catalogação na Fonte: Sistema de Bibliotecas, UFPR
Biblioteca de Ciência e Tecnologia

G629s Golyjeswski, Orides Wladislau
Simulation of thermal stratification using the a 2DV (CE-QUAL-W2) and a 3D (DELFT3D) model. the case study: Passaúna reservoir [recurso eletrônico] / Orides Wladislau Golyjeswsk – Curitiba, 2020.

Dissertação - Universidade Federal do Paraná, Setor de Tecnologia, Programa de Pós-Graduação em Engenharia Ambiental.

Orientador: Tobias B. Bleninger.

1. Modelos hidrodinâmicos – Bidimensionais – Tridimensionais. I. Universidade Federal do Paraná. II. Bleninger, Tobias B. III. Título.

CDD: 532.5

Bibliotecária: Roseny Rivelini Morciani CRB-9/1585

# TERMO DE APROVAÇÃO

Os membros da Banca Examinadora designada pelo Colegiado do Programa de Pós-Graduação em ENGENHARIA AMBIENTAL da Universidade Federal do Paraná foram convocados para realizar a arguição da Dissertação de Mestrado de **ORIDES WLADISLAU GOLYJESWSKI** intitulada: **SIMULATION OF THERMAL STRATIFICATION USING THE A 2DV (CE-QUAL-W2) AND A 3D (DELFT3D) MODEL. THE CASE STUDY: PASSAÚNA RESERVOIR**, que após terem inquirido o aluno e realizada a avaliação do trabalho, são de parecer pela sua APROVAÇÃO no rito de defesa.

A outorga do título de mestre está sujeita à homologação pelo colegiado, ao atendimento de todas as indicações e correções solicitadas pela banca e ao pleno atendimento das demandas regimentais do Programa de Pós-Graduação.

Curitiba, 01 de Setembro de 2020.

Assinatura Eletrônica
02/09/2020 07:48:04.0
TOBIAS BERNWARD BLENINGER
Presidente da Banca Examinadora (UNIVERSIDADE FEDERAL DO PARANÁ)

Assinatura Eletrônica
02/09/2020 09:43:57.0
IRAN EDUARDO LIMA NETO
Avaliador Externo (UNIVERSIDADE FEDERAL DO CEARÁ)

Assinatura Eletrônica
02/09/2020 08:16:28.0
MICHAEL MANNICH
Avaliador Interno (UNIVERSIDADE FEDERAL DO PARANÁ)

## ACKNOWLEDGMENT

Thanks to my family for all the support. Always.

Thanks to my advisor and all the other teachers who helped and taught me so much during this project.

Also, thanks to CAPES for the support. This study was financed in part by the Coordenação de Aperfeiçoamento de Pessoal de Nível Superior - Brasil (CAPES) - Finance Code 001.

## RESUMO

Modelos hidrodinâmicos são ferramentas complexas porém indispensáveis para o gerenciamento e estudo de corpos d'água. Estes modelos podem ser uni, bi ou tridimensionais e podem exigir diversos tipos de condições de contorno para o seu correto funcionamento. Modelos tridimensionais oferecem uma gama maior de resultados e geralmente com qualidade superior porém são extremamente caros em termos computacionais e na aquisição de dados necessários para seu funcionamento; em termos computacionais, modelos bidimensionais oferecem certa vantagem. O objetivo deste trabalho é mostrar que modelos bidimensionais são capazes de representar um reservatório de água sem perder acurácia em seus resultados quando comparados com modelos tridimensionais. Para fazer isso, o reservatório Passaúna foi modelado com o modelos tridimensional Delft3D e com o modelo bidimensional CE-QUAL-W2. Foi possível mostrar que o modelo bidimensional em questão foi capaz de produzir resultados satisfatórios e em alguns casos até mesmo melhores do que o modelo tridimensional, e com custo computacional muito menor, porém nota-se que a utilização dos modelos tridimensionais é mais simples e estes modelos possuem muito mais suporte à ferramentas de pós processamento do que a opção bidimensional.



Palavras-chave: Modelos hidrodinâmicos. Bidimensionais. Tridimensionais.

## ABSTRACT

Hydrodynamic models are complex but indispensable tools for the management and study of water bodies. These models can be uni, bi or three-dimensional and may require several types of boundary conditions for their correct operation. Three-dimensional models offer a wider range of results and are generally of superior quality but are extremely expensive in terms of computation time and data acquisition required; In computational terms, two-dimensional models offer an advantage. The objective of this work is to show that two-dimensional models can represent a water reservoir without losing accuracy in their results when compared to three-dimensional models. To do this, the Passaúna reservoir was modeled with the three-dimensional Delft3D model and the two-dimensional model CE-QUAL-W2. It was possible to show that the two-dimensional model in question was able to produce satisfactory results, and in some cases even better than the three-dimensional model, and with a much lower computational cost. However, it is noted that the use of three-dimensional models is more straightforward, and these models have much more support for post-processing tools than the two-dimensional option.



Keywords: Hydrodynamic models. Two-dimensional. Three-dimensional.

## LIST OF FIGURES

## LIST OF TABLES

## LIST OF ACRONYMS

| | |
|---|---|
| UFPR | Federal University of Paraná |
| SANEPAR | Parana water and waste management company |
| ADCP | Acoustic Doppler Current Profiler |
| ABT | Automated Bubble Trap |
| RANS | Reynolds averaged Navier Stokes |
| FVM | Finite Volume Method |
| FDM | Finite Difference Method |
| BC | Boundary Condition |
| IC | Initial Condition |
| AEM | Algebraic Eddy Viscosity |
| QUICKEST | Quadratic Upstream Interpolation for Convective Kinematics with Estimated Streaming Terms |
| MUDAK | Multidisciplinary Data Acquisition as Key for a Globally Applicable Water Resource Management |
| LARSIM | Large Area Runoff Simulation Model |

## CONTENTS

# 1 INTRODUCTION

Hydrodynamic and heat transport models can be modeled using one, two or three dimensions, with the use of one model in detriment of another being conditioned by the characteristics of the environment to be modeled as well as objectives to be achieved (Ji, 2008). These numerical models are used in the area of water resources because they are more efficient than experimental models (Huang and Ng, 2007) and also allow the development of important scenarios for water resources management and environmental studies.

Water reservoirs for public supply have some basic characteristics such as low speeds, which are mainly controlled by variations in meteorological conditions. The main meteorological variables are wind speed and direction and solar radiation. The great temporal and spatial variation of these parameters makes the use of computational models interesting for the area of water resources management.

One-dimensional models use mean values in two determined dimensions, for example, mean values in the transversal and longitudinal directions or mean values in the transversal and vertical directions. Therefore, these models require that the possible heterogeneity of properties in these directions do not significantly alter the balance of properties in the direction of interest (Bonnet et al., 2000). Computationally speaking, these models are relatively simple and inexpensive to use.

In turn, two-dimensional models use mean values only in one direction: transversal or vertical. Therefore, they present the results in the longitudinal-vertical or longitudinal-transversal planes according to the model used. They require larger amounts of data than one-dimensional models and the quality of the results is conditioned by the quality of the input data (Leopardi et al, 2002). As the balance of all modeled properties is made in two dimensions, much more calculations are made and these models require higher investments in computational power when compared with one-dimensional models (Versteeg and Malalasekera, 2007). Although they require much more processing, they are much simpler than three-dimensional models.

At last, three-dimensional models balance all properties in all directions. This complexity usually limits the use of these models to extremely dynamic and highly stratified environments (Ji, 2008), as they are highly conditioned to the available computational capabilities (USACE, 2010).

The choice of one of the mathematical models available to represent an environment and the interactions with its surroundings depends on several factors, as noted by USACE (2010), Versteeg and Malalasekera (2007), and others. Moreover, different methods can produce different results, so the use of one or more models to represent the same region must be carefully analyzed.

There are several studies comparing one-dimensional models with three-dimensional models and comparisons between one-dimensional models and vertically averaged two-dimensional models are also common. However, studies comparing two-dimensional models and three-dimensional models are rather scarce.

The overall objective of this work is to compare the approach and results of a laterally averaged two-dimensional model with the approach and results of a three-dimensional model. Since two-dimensional models require less computational power, the

aim is to answer whether two-dimensional models are able to produce results similar to the 3D models without significant loss of accuracy.

The specific objective is to assemble the models and work with the various boundary conditions and solve problems inherent to the modeling of water bodies such as uncertainties, data gaps, and inconsistencies in the input data, with particular attention to the water balance of the water body. Additionally, we have to deal with the different formats of data input and output of the models to build a fair comparison between the two results.

In order to achieve this goal, the three-dimensional model Delft3D and the two-dimensional model CE-QUAL-W2 were built for a water distribution reservoir in the city of Curitiba, Paraná, Brazil. The results of the models were compared with each other and with field measurements, with thermal stratification and hydrodynamics as the focus of the analysis.

# 2 THEORETICAL BACKGROUND LITERATURE REVIEW

Regarding the study of water bodies, mechanistic models can be used either as predictive tools or as sources of information on cause-and-effect. Therefore, these models provide a better understanding of water bodies and are important assets to any management program (Martin and McCutcheon, 2018).

## 2.1 MATHEMATICAL MODELS APPLIED TO HYDRODYNAMICS IN LAKES AND RESERVOIRS

Water flow, which controls the quantity and quality of water bodies, is determined by its path, volume and speed. These characteristics are important to the understanding of how water flux and movement alters the concentration of dissolved and suspended materials (Martin and McCutcheon, 2018). Several factors can influence the hydrodynamics of a water body, such as: inflow and outflow characteristics; wind stirring; solar radiation; air temperature and humidity; evaporation; light penetration in the water column; bottom friction; and rain. Figure 2.1 illustrates these factors on a water body. There is extensive research on how and how much each factor influences the dynamics of the water body and there are several models and approaches for each segment. In hydrodynamics studies, the underlying principles used in the derivation of mechanistic models are conservation laws. Conservation of mass is the most basic of these principles, with it being used in the creation of transport models, for mass cannot be created or destroyed; conservation of momentum balances forces and momentums in a system; and conservation of energy allows the formulation of a heat balance for temperature. These laws are dependent on the density of water, which in turn varies with temperature, pressure and concentration of dissolved materials.

### 2.1.1 Equation of state — density as a function of temperature

Density of water as a function of temperature (T ) can be calculated with the Thiesen-Scheel-Diesselhorst equation:

$$\rho(T) = 1000 \left[ 1 - \frac{T + 288.94}{508929.2(T + 68.12963)} (T - 3.9863)^2 \right]. \tag{2.1}$$

Figure 2.2 illustrates the aforementioned variation, with pressure as a constant. Therefore, the density and consequently the temperature of water show an “active behavior” regarding hydrodynamic interference, because its gradient can generate forces in sufficient magnitude to relevantly influence the movement of water (SisBaHiA, 2019).

For seawater, or for applications in which salinity is an important factor, the UNESCO equation of state can be used, which differs from Equation (2.1) by 0.03 °C for $0 < \mathrm{T} < 40$ °C and uses zero salinity (UNESCO, 1981).

In lakes and reservoirs, the difference between the bottom and surface temperature is caused mainly by interactions between the heat absorbed by the water and the wind action on the surface. A thermally stratified lake exhibits three layers:

- Epilimnion – this mixed layer is the top-most layer and, because it is warmer than the rest of the water body, it has a lower density. It is also the region with higher

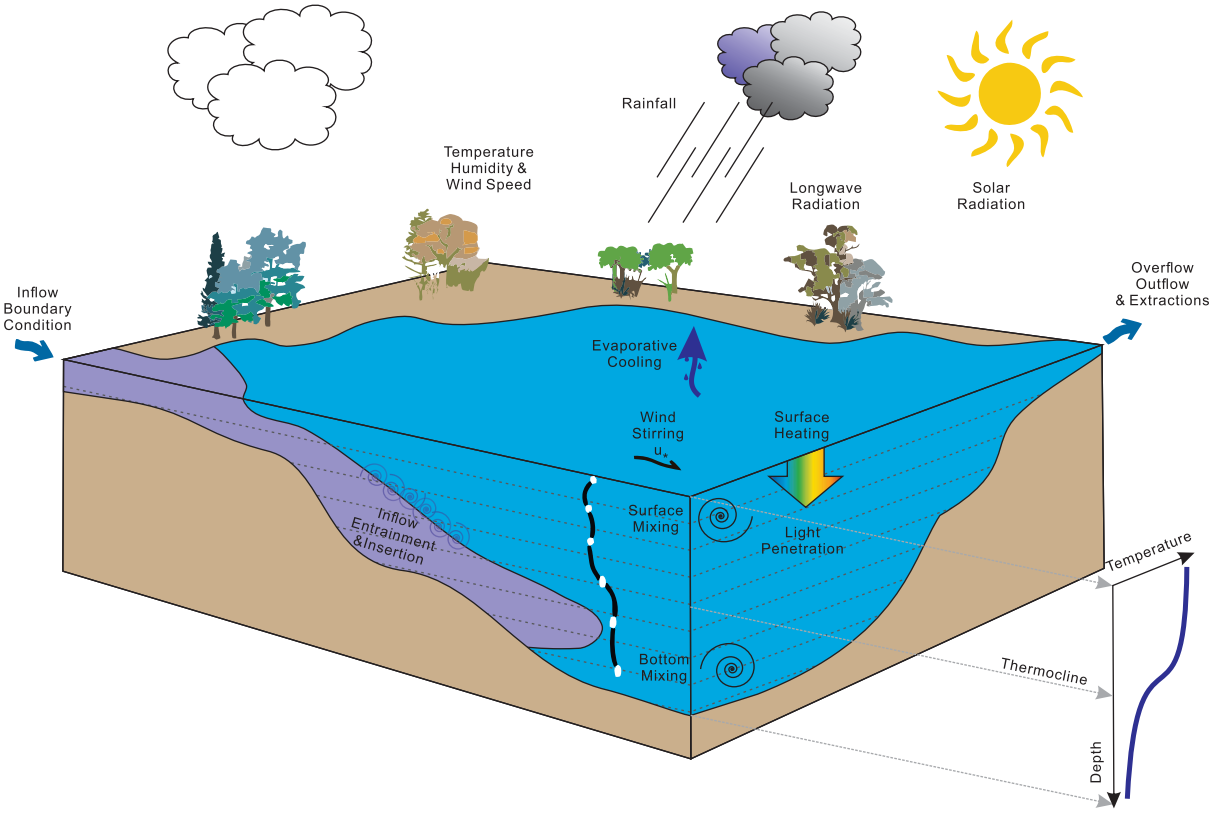


Figura 2.1: The General Lake Model schematization of a generic lake and key processes. Adapted from Hipsey et al. (2019).

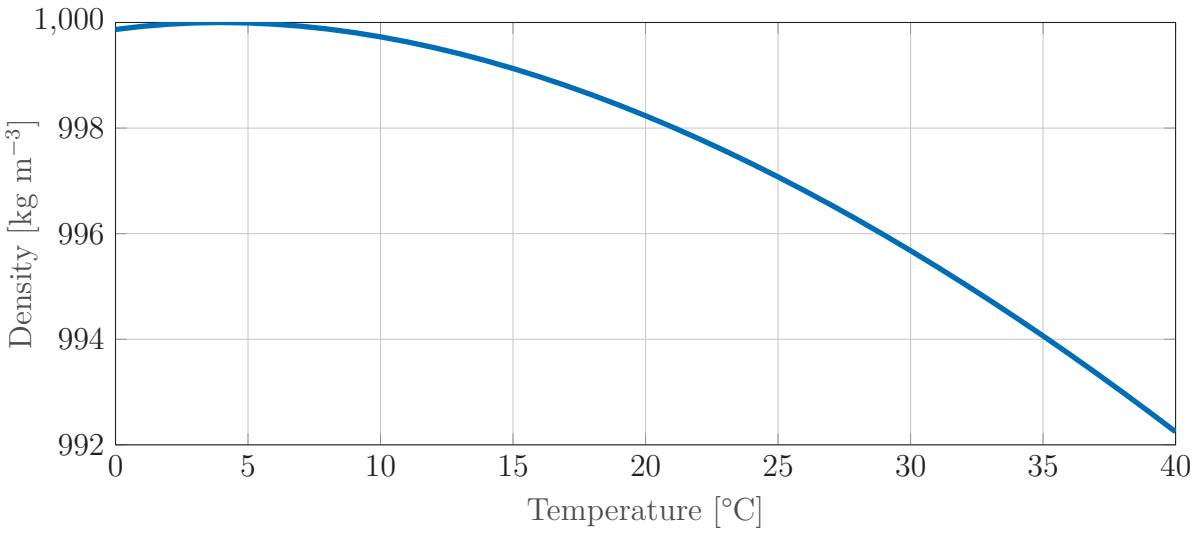


Figura 2.2: Density of water in function of temperature at 1 atm.

concentrations of dissolved oxygen because of wind aeration and because of the Phytoplankton community that tends to stay in this region in search of sunlight.

- Metalimnion – : it is a thin and subtle layer in which the temperature varies more rapidly with the depth of the thermocline, which is not fixed and changes with time. If the lake does not have a thermocline then the water body is well mixed and is essentially isothermal.

- Hypolimnion – it is the bottom layer and is denser and cooler than the rest of the water body. Under extreme conditions this layer may be completely depleted of dissolved oxygen. Nutrient cycling may be impaired under these conditions.

### 2.1.2 Heat balance in lakes and reservoirs

The temperature is measured by the heat content that flows into or out of the water body, which can be exchanged with the atmosphere, water inflows and outflows, and with bed sediment (Niño and Tamburrino, 2004). Typically, only exchanges with the atmosphere are taken into account as it is the most important type of exchange, thus greatly simplifying measurements. The net heat flux from the atmosphere can be calculated by

$$H_n = H_{\text{sw}} + H_H - H_B - H_L - H_s, \tag{2.2}$$

in which $H_{\text{sw}}$ is the heat flux from short-wave solar radiation; $H_H$ is the heat flux from the clouds and the atmosphere, that is, part of the solar radiation, in the form of long-wave radiation, reflected to Earth after being absorbed by the atmosphere and its constituents; $H_B$ is the heat flux from black-body radiation (Stefan-Boltzman's law); $H_L$ denotes heat losses due to evaporation; and $H_s$ corresponds to heat losses due to sensible heat transfer. Each of these fluxes has its empirical relationships and further hypothesis, simplifications and requirements. Vertical heat transport in the water body is calculated by taking into account the penetration of short-wave radiation through the water column and is a function of the depth, the heat flux across the water surface, and the light extinction coefficient which in turn depends on the turbidity and color of the water.

### 2.1.3 Effects of the wind on lakes and reservoirs

Wind tends to mechanically mix the heat added at the surface with the lower layers by exerting a force on the surface of the lake (Lane, 2019). The stress ($\boldsymbol{\tau}_w$) exerted by the wind is usually written as

$$\boldsymbol{\tau}_w = C_D \rho_{\text{air}} |\boldsymbol{u}_w| \boldsymbol{u}_w, \tag{2.3}$$

in which $C_D$ is the drag coefficient; $\rho_{\text{air}}$ is the air density; and $\boldsymbol{u}_w$ is the wind speed 10 m above the water surface. The drag coefficient has values within the range of $1.0 \cdot 10^{-3}$ to $1.5 \cdot 10^{-3}$ (Fischer et al., 2013).

The shear drags the water in the downwind direction, which creates the "surface set-up", a tilted water level. When the wind stops, the potential energy added by this tilting is released, causing standing waves (seiches). Although this inclination is in the order of millimeters in water level, it can cause variations in the order of meters for the isopycnals (Socolofsky and Jirka, 2005). The total force exerted by the wind is equal to the stress ($\boldsymbol{\tau}_w$) multiplied by the superficial area of the reservoir, thus the area of the lake/reservoir and direction of the wind can also change the mixing processes of the reservoirs.

### 2.1.4 Effects of inflows and outflows in lakes and reservoirs

Inflows of reservoirs can be river flow discharges from industries, watershed runoff, and rain. These discharges act as boundary conditions for the reservoir and greatly change

the lake dynamics. If there is no density difference between the inflow water and the reservoir water, the mixing process is local and almost instantaneous. Otherwise, the inflow will create a density current in the form of overflow, interflow or underflow depending of the buoyancy of the intruding water.

Outflows can be natural releases from the lake or discharges from a reservoir spillway. The volume of water flowing out of the reservoir changes the water balance of the lake and affect water surface elevation, surface area and total volume. The release of water converts one form of energy into another (potential energy into kinetic energy), which favors the mixing (Ji, 2008).

## 2.2 MODELING THE HYDRODYNAMICS AND PASSIVE SCALAR TRANSPORT OF LAKES AND RESERVOIRS

Several models can be applied in lakes and reservoirs according to the expected objectives and phenomena of interest. Hydrodynamic and transport models can solve the equations of conservation of mass, momentum, and energy.

Hydrodynamic models can be one, two or three-dimensional in scale depending on the scale of interest. It is possible to analyze the steady, unsteady and gradually varied conditions by numerically solving the equations of continuity, momentum, and scalar transport.

### 2.2.1 Coordinate system and grid systems

Engineering solutions almost always require the definition of a convenient coordinate system that better suits the characteristics of the problem at hand. Two sets of commonly used coordinates in simulation studies of water bodies are shown below.

#### *2.2.1.1 $\sigma$-coordinate system*

In order to obtain a smooth representation of the bathymetry and a uniform resolution in the vertical direction (Ji, 2008), the $\sigma$-coordinate system can be defined by

$$\sigma = \frac{z-\zeta}{d+\zeta} = \frac{z-\zeta}{H}, \tag{2.4}$$

in which $z$ is the vertical coordinate in the physical space; $\zeta$ is the free surface elevation above the reference plane (at $z = 0$); $d$ is the depth below the reference plane; and $H$ is the total water depth. Figure 2.3 shows a schematization of this coordinate system, and Figure 2.4 shows the $\sigma$ and $z$ coordinate system applied to a generic water body.

#### *2.2.1.2 z-coordinate system*

The discretization accuracy of the vertical processes is determined by the vertical grid system (Deltares, 2014). The $\sigma$-coordinate system does not always have enough resolution around the pycnoclines, thus it can generate significant errors in areas with horizontal density gradients and steep bottom bathymetry (Deltares, 2014).

The $z$-coordinate system is not limited by the real boundary in the vertical direction. The free surface and bottom of the lake is represented in a staircase fashion, as shown in Figure 2.4(b). This representation may lead to inaccuracies of the bed stress and

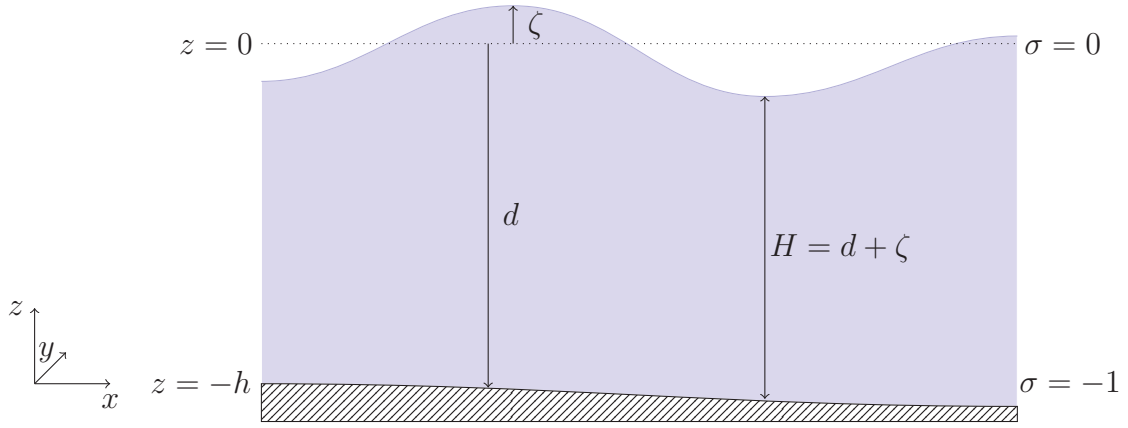


Figura 2.3: Definition of water level ($\zeta$), depth ($h$) and total depth ($H$) in the sigma coordinate system.

water level, but it can better represent the isopycnals in areas with steep bottom slopes (Deltares, 2014).

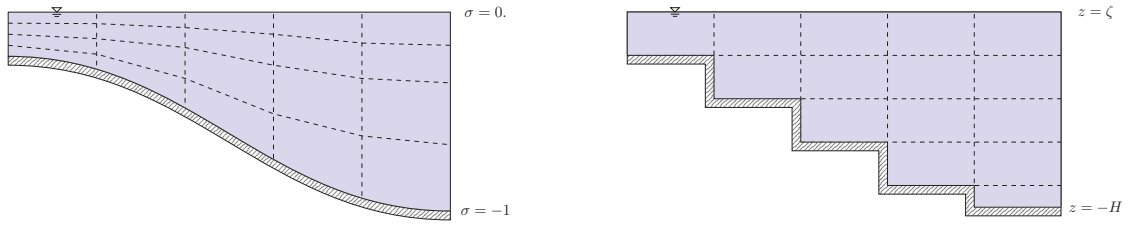


(a) (b)

Figura 2.4: (a) $\sigma$-coordinate system. (b) $z$-coordinate system. Note the number of volumes of the computational grid.

In the $\sigma$-coordinate system, the number of layers over the entire computational area is constant, thus making this set of coordinates computationally more expensive than those of the $z$-coordinate system in which the layer thickness does not necessarily need to be constant, allowing better resolutions in specified zones of interest. In deeper regions, the density stratification may be better modeled by the $z$-coordinate system because the grid distribution in the vertical direction is more or less parallel to the isopycnals. Since the $\sigma$-coordinate system follows the local bathymetry, it may not be completely parallel to the isopycnals and will lead to more numerical diffusion and worst results. However, in shallow regions, the lack of computational cells in the $z$-system greatly mixes, in a numerical way, the water in that region. Such problem does not exist in the $\sigma$-system due to the fixed number of computational cells. Underflows are also underrepresented in the z-coordinate system since the bottom has a staircase form. Due to the aforementioned aspects, the $z$-coordinate system is better suited for studies of density stratification of reservoirs in deeper regions, while the $\sigma$-coordinate system is better suited for studies of density currents.

#### *2.2.1.3 Curvilinear grid*

In the longitudinal-transversal direction, a curvilinear grid, also called "body-fitted" grid, is possible. They provide geometric flexibility and are able to better represent the geometry of the system as shown in Figure 2.5, in which the rectangular and curvilinear

grid systems are applied to the Passaúna reservoir. Note that, in this case, the grid is also locally refined to better represent the characteristics of the horizontal boundaries.

However, these grids are difficult to create and are time-consuming. The formulation of the equations of momentum, mass, energy, and scalar conservation are much more complex and some transformations are required for the solving algorithm to work properly (Versteeg and Malalasekera, 2007).

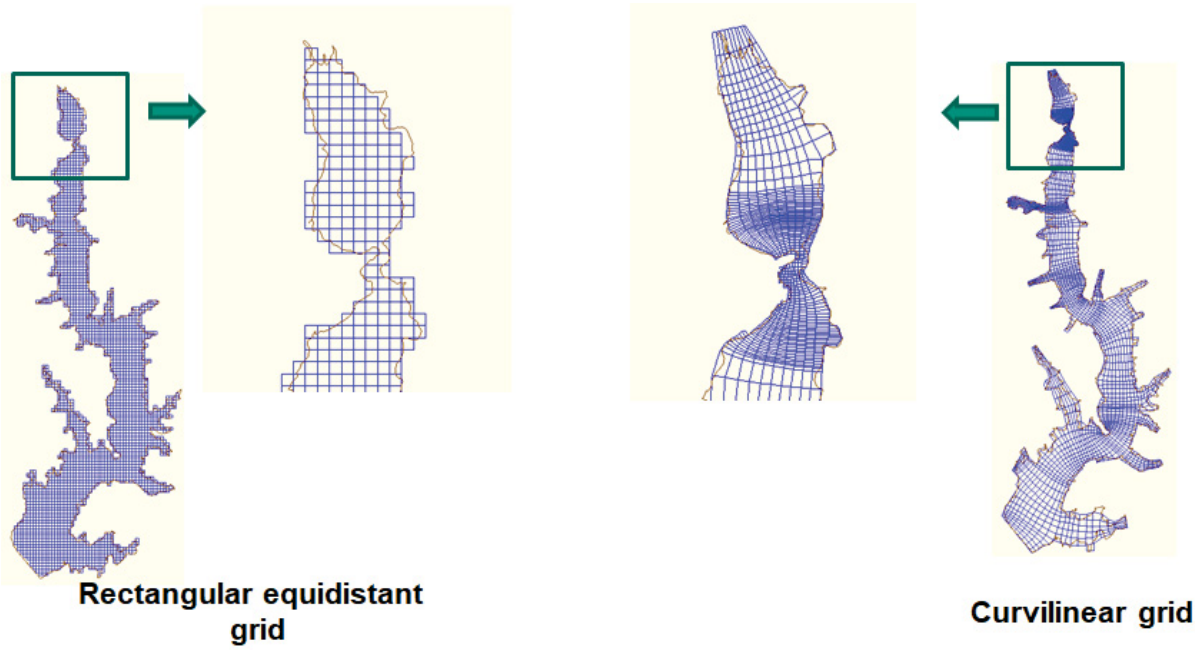


Figura 2.5: Examples of the rectangular and curvilinear grid systems applied to the Passaúna reservoir.

### 2.2.2 Three-dimensional models

Every flow is three-dimensional by nature and, when described mathematically, a set of 5 differential equations are created: one for the continuity, three for each spatial direction ($x$, $y$ and $z$ — or $\sigma$) of the conservation of momentum, and one for the energy conservation. These equations rarely have an analytical solution, which demands the use of simplifications and, almost always, numerical solutions.

Starting from the Navier-Stokes equations of motion and assuming a Boussinesq approximation[1], hydrostatic pressure[2], and Reynolds decomposition we can get a simplified form of the equations of motion in three-dimensions: the shallow water formulation. The following descriptions use definitions of the Delft3D model for simplicity (Deltares, 2014). Using the $\sigma$-coordinate system, the continuity equation yields

$$\frac{\partial \zeta}{\partial t} + \frac{\partial (d+\zeta)u}{\partial x} + \frac{\partial (d+\zeta)v}{\partial y} + \frac{\partial (d+\zeta)w}{\partial \sigma} = Q, \tag{2.5}$$

in which $u, v$ and $w$ are the fluid velocity components in the $x, y$ and $z$ coordinates, respectively; and $Q$ is the global source or sink per unit of area (m s$^{-1}$). For the conservation of momentum we have

[1]Density variation is only important in the buoyancy term ( $\rho \boldsymbol{g}$) and can be left unattended in the rest of the equation.

[2]When shallow water assumption is valid, vertical accelerations are assumed to be small compared to the gravitational acceleration and are therefore not taken into account.

$$\frac{\partial u}{\partial t} + u\frac{\partial u}{\partial x} + v\frac{\partial u}{\partial y} + \frac{w}{d+\zeta}\frac{\partial u}{\partial \sigma} - fv =$$
$$M_x - \frac{1}{\rho}\frac{\partial p}{\partial x} + \frac{1}{(d+\zeta)^2}\frac{\partial}{\partial \sigma}\left(\nu_v \frac{\partial u}{\partial \sigma}\right) + \nu_h\left(\frac{\partial^2 u}{\partial x^2} + \frac{\partial^2 u}{\partial y^2}\right), \tag{2.6}$$

$$\frac{\partial v}{\partial t} + u\frac{\partial v}{\partial x} + v\frac{\partial v}{\partial y} + \frac{w}{d+\zeta}\frac{\partial v}{\partial \sigma} - fu =$$
$$M_y - \frac{1}{\rho}\frac{\partial p}{\partial y} + \frac{1}{(d+\zeta)^2}\frac{\partial}{\partial \sigma}\left(\nu_v \frac{\partial v}{\partial \sigma}\right) + \nu_h\left(\frac{\partial^2 v}{\partial x^2} + \frac{\partial^2 v}{\partial y^2}\right) \tag{2.7}$$

and

$$\frac{\partial p}{\partial \sigma} = -\rho g h \tag{2.8}$$

in which $u, v$ and $w$ are the velocities in $x, y$ and $\sigma$ direction, respectively; $f$ is the Coriolis parameter ($s^{-1}$); $M_x$ and $M_y$ are the depth-averaged mass fluxes due to Stokes drift (kg m $s^{-1}$) in $x$ and $y$ direction, respectively; $p$ is the hydrostatic water pressure (kg $m^{-1}$ $s^{-2}$); and $\nu_h$ and $\nu_v$ are the vertical and horizontal eddy viscosity ($m^2$ $s^{-1}$). Finally, for the conservation of energy we have

$$\frac{\partial (d+\zeta)T}{\partial t} + \frac{\partial (d+\zeta)uT}{\partial x} + \frac{\partial (d+\zeta)vT}{\partial y} + \frac{\partial (wT)}{\partial \sigma} = (d+\sigma)\left[\frac{\partial}{\partial x}\left(D_H \frac{\partial T}{\partial x}\right)\right] +$$
$$+(d+\sigma)\left[\frac{\partial}{\partial y}\left(D_H \frac{\partial T}{\partial y}\right)\right] + \frac{1}{d+\zeta}\frac{\partial}{\partial \sigma}\left(D_V \frac{\partial T}{\partial \sigma}\right) + \frac{1}{\rho c_p} S, \tag{2.9}$$

in which $T$ is the water temperature (°C); $D_H$ and $D_V$ are the horizontal and vertical eddy diffusivity coefficients ($m^2$ $s^{-1}$), respectively; and $S$ is a source or sink term per unit area due to discharge (W $m^{-1}$).

To get a well-posed mathematical problem with a unique solution, an appropriate set of initial (IC) and boundary conditions (BC) for water levels, temperature distributions and horizontal velocities must be specified (Deltares, 2014). The IC and BC need to be set and are often critical for the performance of the model (Ji, 2008). Since we cannot model outside the water body domain, the initial conditions specify the state of the water body at the beginning of the simulation and the boundary conditions specify the features on the borders of the computational space.

Boundary conditions include vertical boundary conditions and horizontal boundary conditions (Figure 2.6). The Equations (2.5) to (2.8) require five BC and (2.9) requires six BC.

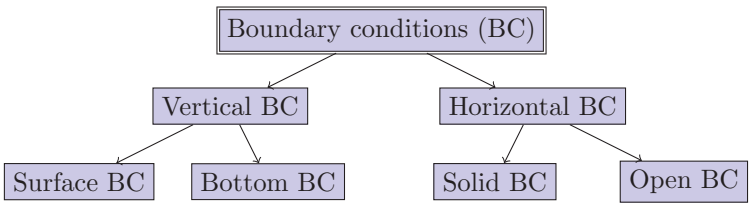


Figura 2.6: Existing boundary conditions required for application of mathematical models.

For the solid horizontal BC, the velocity must be tangential to the boundary since there is no flux through it, or

$$v_n = 0. \tag{2.10}$$

For any scalar (temperature, salinity, pollutant, etc.) $c$ the solid boundary conditions can be written as

$$\frac{\mathrm{d}c}{\mathrm{d}n} = 0, \tag{2.11}$$

where $n$ is the coordinate normal to the boundary. For the momentum equations the bed BC can be written as

$$\left.\frac{\nu_v}{H}\frac{\partial u}{\partial \sigma}\right|_{\sigma=-1} = \frac{1}{\rho_0}\tau_{b\xi} \tag{2.12}$$

and

$$\left.\frac{\nu_v}{H}\frac{\partial v}{\partial \sigma}\right|_{\sigma=-1} = \frac{1}{\rho_0}\tau_{b\eta}, \tag{2.13}$$

in which $\tau_{b\xi}$ and $\tau_{b\eta}$ are the bed stress at the $\xi$ and $\eta$ direction, respectively.

Horizontal open boundaries are virtual "water-water" boundaries (Deltares, 2014) through which flow can cross without obstruction or reflections. For those BC, the water level and the normal velocity, or a combination of the two should be prescribed. It is also possible to define many other formulations to solve problems of the required boundary conditions.

For the turbulence closure models, Delft3D offers four alternatives: a constant coefficient specified by the user; Algebraic Eddy viscosity closure Model (AEM), in which algebraic is used to determine the turbulent kinetic energy ($k$) and mixing length ($L$); $k$–$L$ model, in which transport equations are solved for $k$ and the $L$ is calculated in the same way as the AEM model; and $k$–$\epsilon$, in which two transport equations are solved: one for the turbulent kinetic energy and one for the dissipation rate of the turbulent kinetic energy ($\epsilon$).

The Delft3D model uses a cell-centred finite difference method for the discretization of the above mentioned equations and uses, in the time integration, a implicit scheme Deltares (2014) allowing larger time steps.

### 2.2.3 Two-dimensional models

Two-dimensional models are three-dimensional models mediated in any direction. The differential equations for conservation of momentum, mass, and energy can be integrated on the transversal or vertical direction depending on the hypotheses considered and their applications change from case to case.

The vertical integration generates 2DH models, in which the vertical component is averaged, that is, integrated into that direction for the horizontal distribution of properties (results in the $xy$ plane) to be obtained. This approach is better suited when the variation of the properties in the vertical direction is smaller than their variations in the horizontal direction. Broad, well-mixed and shallow water bodies can be well represented with vertically averaged 2D models.

The horizontal integration of three-dimensional equations generates 2DV models, in which the variation in the transversal direction is considerably smaller than in the vertical direction. This version of the equations provides us with results in the $xz$ plane.

The 2DV model CE-QUAL-W2 solves equations of continuity and momentum, which are listed below.

$$\frac{\partial uB}{\partial x} + \frac{\partial wB}{\partial z} = qB, \tag{2.14}$$

is the continuity equation, in which $u$ and $w$ are the velocity components; $B$ is the cross-sectional width; and $q$ is the net lateral inflow per unit of volume.

$$\frac{\partial uB}{\partial t} + \frac{\partial uuB}{\partial x} + \frac{\partial uwB}{\partial z} = gB\sin\alpha - \frac{B}{\rho}\frac{\partial p}{\partial x} + \frac{1}{\rho}\frac{\partial B\tau_{xx}}{\partial x} + \frac{1}{\rho}\frac{\partial B\tau_{xz}}{\partial z} \tag{2.15}$$

and

$$\frac{1}{\rho}\frac{\partial p}{\partial z} = g\cos\alpha \tag{2.16}$$

are the momentum equations, in which $t$ is the time; $g$ is the gravitational acceleration; $\alpha$ is the channel slope; $\rho$ is the water density; $p$ is the pressure; and $\tau_{xx}$ and $\tau_{xz}$ is the shear stress in the the x and z coordinates.

Figure 2.7 shows a schematization of a water body with the basic variables, namely, width and cross-sectional area of the cells and distance between adjacent cross-sections, and the coordinate system adopted for 2DV models.

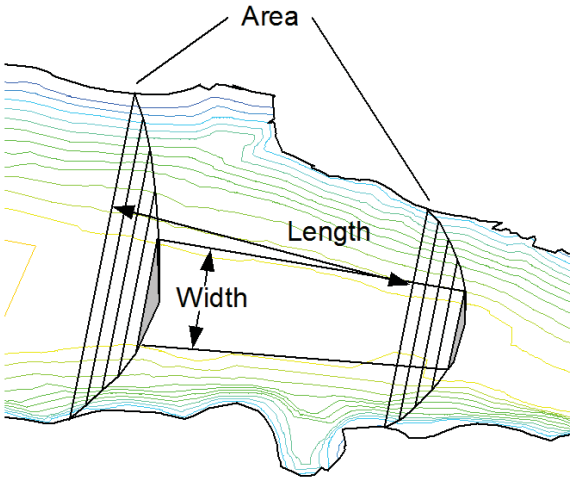


Figura 2.7: Basic variables of the bathymetry used in a two-dimensional horizontally integrated model.

The equation of the free surface elevation is

$$B_\eta\frac{\partial \eta}{\partial t} = \frac{\partial}{\partial x}\int_\eta^h uB\mathrm{d}z - \int_\eta^h qB\mathrm{d}z \tag{2.17}$$

in which $\eta$ is the free water surface elevation. This equation is also required for the iterative solution process, which is conducted as follows: the equation (2.17) is solved with IC and BC, followed by the solution of Equation Equation (2.15) for $u$ and Equation (2.14) for $w$. With the hydrodynamics complete, Equation (2.18) is solved and, finally, the density field is calculated with Equation (2.1).

where $\eta$ is the free water surface elevation. This equation is also needed for the iterative process of the solution. The iterative solution process is as follows: with

BC and IC the equation (2.17) is solved folowed by the solution of Equation 2.15 for $u$ and Equation 2.14 for $w$. With the hydrodynamics complete, the advective-diffusive Equation 2.18 is solved and finally the density field is calculated with the Equation of state (2.1).

The heat transfer is modeled by

$$\frac{\partial BT}{\partial t}+\frac{\partial uBT}{\partial x}+\frac{\partial wBT}{\partial z}=\frac{\partial}{\partial x}\left(BD_x\frac{\partial T}{\partial x}\right)+\frac{\partial}{\partial z}\left(BD_z\frac{\partial T}{\partial z}\right)+\frac{1}{\rho c_p}q_T B+\frac{1}{\rho c_p}S_T B, \quad (2.18)$$

in which $T$ is the temperature; $D_x$ and $D_z$ are the longitudinal and vertical temperature dispersion coefficients; $q_T$ is the lateral inflow or outflow mass flow rate per unit volume; and $S_T$ is the laterally averaged source/sink term.

The vertical shear stress boundary condition for the bottom of the water-body can be calculated using

$$\tau_b=\frac{\rho_w g}{C^2}u|u|, \quad (2.19)$$

in which $C$ is the Chezy coefficient. The vertical shear stress surface BC is calculated by Equation (2.3). For the heat transfer equation, the boundary conditions are: the heat exchange with the atmosphere (surface BC — Equation (2.2)) and heat exchange with the bottom ($H_\mathrm{b}$) which can be calculated by

$$H_\mathrm{b}=-k_\mathrm{b}(T-T_\mathrm{b}), \quad (2.20)$$

in which $k_\mathrm{b}$ is the heat exchange coefficient; $T$ is the water temperature; and $T_b$ is the sediment bed temperature. A similar equation is used for air temperature.

Table 2.1 shows a summary of the equations used by 3D models, specifically Delft3D with $\sigma$-coordinate system, and 2D models, specifically CE-QUAL-W2 with $z$-coordinate system.

### 2.2.4 One-dimensional models

One-dimensional models are two-dimensional models averaged in any direction. Another integration of the set of equations is made so we can find simpler versions of the conservation laws. These models have been widely used to simulate the quality of water and to calculate the heat balance in reservoirs.

In reservoirs, for which the water velocity is small enough to use $u \approx 0$, only the heat transport in the vertical direction is solved. Figure 2.8 shows the schematization of a one-dimensional model described by Polli (2014). In her model, $U(t)$ is the wind velocity (m s$^{-1}$), $K_H$ is the turbulent diffusion coefficient (m$^2$ s$^{-1}$), $A(z)$ is the superficial area of the reservoir, $q(z)$ is the heat source from the absorption of solar radiation in the water column (J m$^{-2}$ s$^{-1}$), $c_p$ the specific heat capacity of the water (J kg$^{-1}$ K$^{-1}$), $q_n$ is the flow of heat on the surface (J m$^{-2}$ s$^{-1}$) and $H(t)$ is the depth of water (m).

Other notable world wide used one-dimensional models are the DYRESM — Dynamics Reservoir Simulation Model; WASP - Water Quality Analysis Simulation Program; EFDC — Environmental Fluid Dynamics Code.

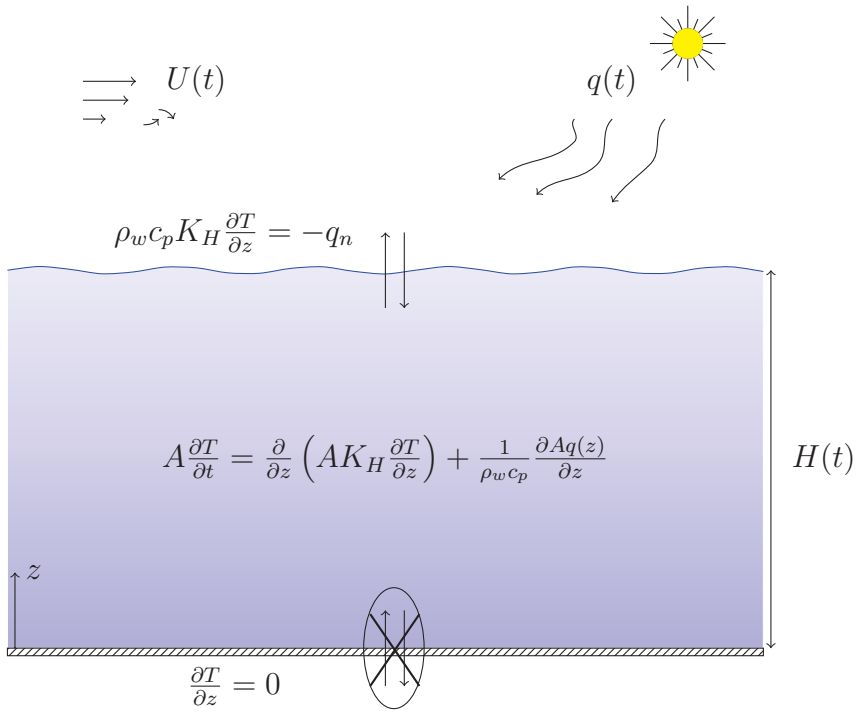


Figura 2.8: Schematisation of a one-dimensional temperature model. Adapted from Polli (2014).

Tabela 2.1: Set of equations solved by 2D model CE-QUAL-W2 and 3D model Delft3D.

| **Model** | **Equation** |
|---|---|
| 2D Continuty | $\frac{\partial uB}{\partial x} + \frac{\partial wB}{\partial z} = qB$ |
| 2D momentum $x$ | $\frac{\partial uB}{\partial t} + \frac{\partial uuB}{\partial x} + \frac{\partial uwB}{\partial z} = gB\sin\alpha - \frac{B}{\rho}\frac{\partial p}{\partial x} + \frac{1}{\rho}\frac{\partial B\tau_{xx}}{\partial x} + \frac{1}{\rho}\frac{\partial B\tau_{xz}}{\partial z}$ |
| 2D momentum $z$ | $\frac{1}{\rho}\frac{\partial p}{\partial z} = g\cos\alpha$ |
| 2D energy | $\frac{\partial BT}{\partial t} + \frac{\partial uBT}{\partial x} + \frac{\partial wBT}{\partial z} - \frac{\partial}{\partial x}\left(BD_x\frac{\partial T}{\partial x}\right) - \frac{\partial}{\partial z}\left(BD_z\frac{\partial T}{\partial z}\right) = \frac{1}{\rho c_p}q_T B + \frac{1}{\rho c_p}S_T B$ |
| 3D Continuty | $\frac{\partial \zeta}{\partial t} + \frac{\partial (d+\zeta)u}{\partial x} + \frac{\partial (d+\zeta)v}{\partial y} + \frac{\partial (d+\zeta)w}{\partial z} = Q$ |
| 3D momentum $x$ | $\frac{\partial u}{\partial t} + u\frac{\partial u}{\partial x} + v\frac{\partial u}{\partial y} + \frac{w}{d+\zeta}\frac{\partial u}{\partial \sigma} - fv = M_x - \frac{1}{\rho}\frac{\partial p}{\partial x} + \frac{1}{(d+\zeta)^2}\frac{\partial}{\partial \sigma}\left(\nu_v\frac{\partial u}{\partial \sigma}\right) + \nu_h\left(\frac{\partial^2 u}{\partial x^2} + \frac{\partial^2 u}{\partial y^2}\right)$ |
| 3D momentum $y$ | $\frac{\partial v}{\partial t} + u\frac{\partial v}{\partial x} + v\frac{\partial v}{\partial y} + \frac{w}{d+\zeta}\frac{\partial v}{\partial \sigma} - fu = M_y - \frac{1}{\rho}\frac{\partial p}{\partial y} + \frac{1}{(d+\zeta)^2}\frac{\partial}{\partial \sigma}\left(\nu_v\frac{\partial v}{\partial \sigma}\right) + \nu_h\left(\frac{\partial^2 v}{\partial x^2} + \frac{\partial^2 v}{\partial y^2}\right)$ |
| 3D momentum $z$ | $\frac{\partial p}{\partial \sigma} = -\rho g h$ |
| 3D energy | $\frac{\partial (d+\zeta)T}{\partial t} + \frac{\partial (d+\zeta)uT}{\partial x} + \frac{\partial (d+\zeta)vT}{\partial y} + \frac{\partial (wT)}{\partial \sigma} = (d+\sigma)\left[\frac{\partial}{\partial x}\left(D_H\frac{\partial T}{\partial x}\right)\right] + (d+\sigma)\left[\frac{\partial}{\partial y}\left(D_H\frac{\partial T}{\partial y}\right)\right] + + \frac{1}{d+\zeta}\frac{\partial}{\partial \sigma}\left(D_V\frac{\partial T}{\partial \sigma}\right) + \frac{1}{\rho c_p}S$ |

## 2.3 LATERALLY AVERAGE MODELING — CE-QUAL-W2 OVERVIEW

Laterally averaged models or 2DV models are based on RANS equations and are commonly used for physically modeling the tidal propagation, hydrodynamics, water quality, and density stratification in lakes, reservoirs, and estuaries, for which the lateral dimension of the water body is small or unimportant compared to the longitudinal dimension.

These models allow the use of a finer resolution in the longitudinal and vertical directions in comparison to 3D models. Also, the laterally averaged approach provides a much cheaper model in terms of computational effort, which in turn provides simulations over a longer time scale than corresponding 3D models (Kurup et al., 2000).

CE-QUAL-W2 is a 2DV model that, since 1975, has been under continuous development. The original model was created by the US Army Corps of Engineers (USACE) with the name LARM — Laterally Averaged Reservoir Model. In 1984, the model was handed over to a team led by Tom Cole, to which major refinements in hydrodynamics and water quality components were added and the name CE-QUAL-W2 was created (Cole and Buchak, 1995). The model is now developed by the Water Quality Research Group at the Portland State University, Oregon, USA.

It is an open-source Eulerian model software that uses a bathymetric map as a geometry input and short-wave radiation, cloud cover, air temperature, dew point temperature, wind speed, wind direction, and precipitation as meteorological inputs. Output data includes water temperature, hydrodynamics, dissolved/particulate solids, dissolved oxygen, nutrients, organic matter, and algae concentration. The calibration parameters are: longitudinal eddy viscosity, longitudinal eddy diffusivity, Manning's roughness coefficient, wind sheltering coefficient, dynamic shading coefficient, the fraction of incident solar radiation absorbed at the water surface, and the light extinction of the water.

The numerical solution of the laterally integrated Navier-Stokes equations used in CE-QUAL-W2 is achieved by the implementation of the QUICKEST numerical method, which is an explicit, third-order finite volume method (Versteeg and Malalasekera, 2007) first introduced by Leonard (1979). This numerical method greatly reduces the numerical diffusion inherent to numerical solutions of PDEs (Versteeg and Malalasekera, 2007) and it was developed to solve a predominantly convective and unsteady flow problem Leonard (1979). When strong gradients are present, the numerical diffusion can be greater than the physical diffusion, which leads to inaccurate results.

To solve the turbulence closure problem, CE-QUAL-W2 offers six options: Nickuradse, RNG, parabolic, W2, W2N, and TKE. W2 and W2N are recommended for water bodies with deep sections that could be stratified and the other options are recommended for rivers and estuary systems (Polli, 2018). W2 solves one equation for the eddy viscosity and assumes the layer thickness as the mixing length, and W2N solves one equation for the eddy viscosity and the mixing length is calculated by the Nickuradse model.

Since its first release in 1975, 2378 studies were reported using the CE-QUAL-W2 model (Portland, 2019) and it is used to model reservoirs, lakes, estuaries, rivers and pit lakes worldwide. Table 2.2 shows the number of papers published by country.

This model has been used to provide information on hydrodynamics and water quality, algae control (Dutta and Das, 2020), simulation of thermal stratification and salt intrusion (Sabeti et al., 2017), and dynamics of reservoirs that are extremely polluted with metals and sulfides (Torres et al., 2016).

Tabela 2.2: Number of works by country that uses the CE-QUAL-W2 model. Source: Portland (2019).

| Country | Number |
|---|---|
| USA | 783 |
| Korea | 232 |
| Canada | 152 |
| Iran | 124 |
| Brazil | 123 |
| China | 116 |
| Portugal | 39 |
| Rest of the world | 809 |
| Total | 2378 |

In Brazil, the model was used in the evaluation and prediction of evaporation and water quality of reservoirs in different regions, showing the versatility of the model. Works such as those carried out by de Farias Mesquita et al. (2020), Conterato et al. (2016), Pion (2018), Gastaldini et al. (2004) and Barros (2019) are good examples of this type of study. Figure 2.9 shows an example of the quality of the results obtained by CE-QUAL-W2, where the model can correctly simulate the variations of the water temperature of a reservoir.

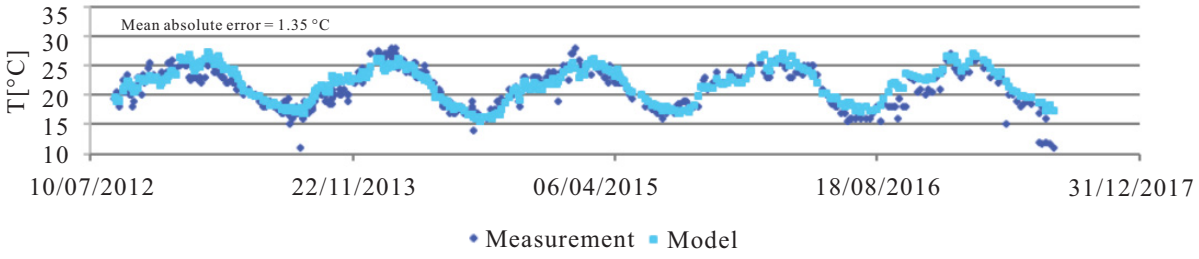


Figura 2.9: Example of result obtained by the CE-QUAL-W2 model: Water temperature at a fixed depth. Adapted from Pion (2018).

Recent studies apply the CE-QUAL-W2 model to estimate changes in water quality as a function of the increase in the flow of the dam Lindenschmidt et al. (2019), or to build submerged barriers to control the flow of water with inadequate temperatures, in an attempt to mitigate the impact of temperature in the downstream sections of the reservoir (Yang et al., 2019; He et al., 2017). These studies show that the CE-QUAL-W2 model has potential to be used in innovative engineering projects. CE-QUAL-W2 is considerably easy to calibrate and even allows the application of neural networks in its calibration, given the extra time needed for its execution, as shown by Ostfeld and Salomons (2005) and Afshar et al. (2011).

## 2.4 DELFT3D

Delft3D is a well documented open-source software with several applications and simulations of the most diverse water bodies. It is a model capable of providing information on hydrodynamics, water quality and sediment transport by simulating the resulting

transport phenomena from meteorological forces, tides and tributary flows (Deltares, 2014). The software was developed by Deltares in partnership with Delft University of Technology in Delft, South Holland, Netherlands. The validation of the computational model based on comparisons between numerical and analytical solutions is shown by Gerritsen et al. (2008).

The model solves the Reynolds-averaged Navier-Stokes (RANS) equations in their three-dimensional form using the shallow water hypothesis and the Boussinesq assumptions. It uses a finite difference scheme as numerical method and accepts both rectangular and curvilinear grids as computational grid, as well as the $\sigma$ and $z$ coordinate systems.

As the CE-QUAL-W2, this model has been used as a predictive tool with flow simulation. It can also be used to identify possible point or diffuse sources of contaminants (Kaçıkoç and Beyhan, 2014) and to study complex irrigation systems (Theol et al., 2019) as well as river morphology evolution (Angamuthu et al., 2018).

In Brazil it has been used in the study of the evolution of river morphology through hydraulic controls, as described by Tomas (2014); hypothetical studies of oil spills in ports (Poletto, 2013); evaluation of plumes of contaminants from submarine outfalls (Ferreira, 2019) and dozens of other water quality studies like Pereira (2003), Falkenberg (2009), Nascimento (2019) and Yang and Harari (2016).

## 2.5 COMPARISONS BETWEEN MODELS

Recent advances in available processing machines led to an increase in the complexity of the models, so that the choice of parameters and dimensionality requires a large degree of expertise from users as well as the applicability of studies that show the ability of 1D, 2D and 3D models to reproduce the evolution of a system. Comparisons between models with different dimensions are conducted to show the advantages of one model over another (Cox, 2010), but the coupling, in order to overcome the drawbacks of different approaches, is more common.

Literature shows that results from 3D models are usually better than those from 2D models for hydraulic applications, as noted by Kasvi et al. (2015). However, the computational effort required by 3D models can make them impossible to use or introduces too many uncertainties in the results (Sousa, 2010).Although errors tend to decrease as the complexity of the mathematical model increases, there is an increase in the sensitivity of the results due to the new variables inserted (Lindenschmidt, 2006), thus, there is a need to evaluate the models' uncertainties and results more carefully before using its results.

Generally, only two-dimensional depth-averaged models are compared with three-dimensional models, in order to evaluate the ability of the 2DH models to predict floods and their evolution. This is mainly because when creating maps of extreme events of flood there is no need for information about the vertical direction. The speed on which is possible to obtain information is also relevant in these topics.

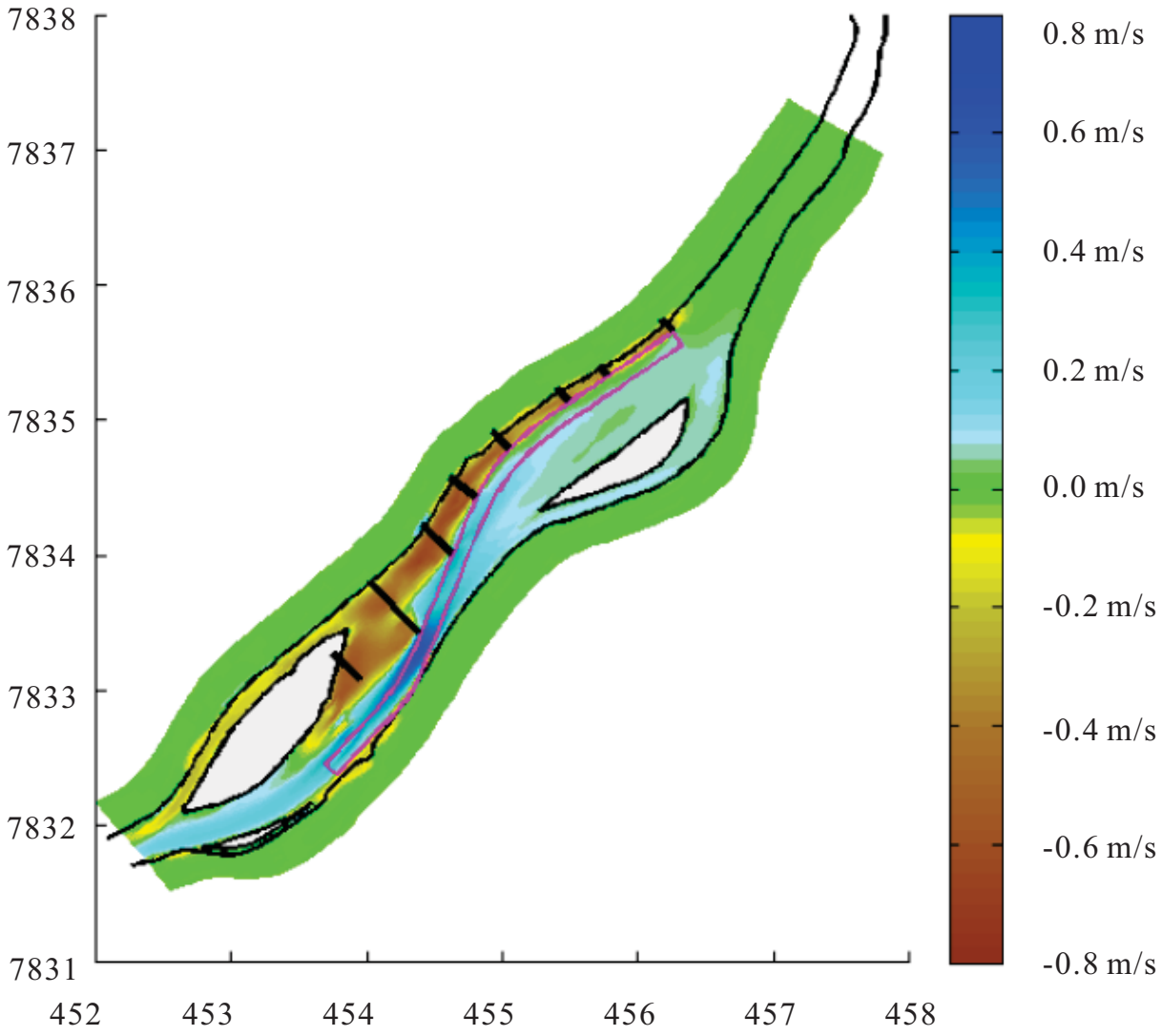


Figura 2.10: Example of result obtained by the Delft3D model: hydraulic control of flows in a stretch of the Paraguay River through the use of groins on the Paraguay River Waterway. Adapted from Tomas (2014).

# 3 MATERIALS AND METHODS

Two computational models were implemented for the Passaúna reservoir during periods of data availability. The study site is described in section 3.1, the 3D computational model in section 3.3 and the 2D computational model in section 3.4.

## 3.1 STUDY SITE: PASSAÚNA RESERVOIR

The Passaúna reservoir, located in the hydrographic basin of the Iguaçu River in the first Plateau of Paraná, is in operation since 1990. The reservoir borders the municipalities of Curitiba, Araucária, and Campo Largo (Paraná State, southern Brazil, see Figure 3.1). Approximately 930 meters above sea level, the region has humid subtropical weather: during the summer the daily average temperature is around 20 °C and in the winter is around 13 °C.

The reservoir has a surface area of about 11 $km^2$, maximum depth of 16 m, and volume of 71.6 $\times 10^2$ $m^3$ (Polli, 2018). Residence time can be estimated to be around 220 days[1]. According to Polli (2018), thermal stratification occurs in the deeper parts of the reservoir during warm periods (September – March) and anoxic conditions may also occur.

### 3.1.1 Inflows and water temperature

Because the measured data for inflows and temperatures had too many gaps, the discharge was modeled and provided by HYDRON, a MUDAK-WRM[2] project partner using the LARSIM model which has identified 64 tributaries (see Figure 3.2 for its locations). Out of these 64 tributaries, there are only two consisted of perennial rivers: the Passaúna River with average discharge of 2.10 $m^3 s^{-1}$ and the Ferraria river with 0.15 $m^3 s^{-1}$ average (see Figure 3.1). The other tributaries consisted of intermittent streams with very low discharge (0 – 0.05 $m^3 s^{-1}$). Figure 3.3 shows the results for daily discharge and temperature for the calibrated and validated LARSIM model for the Passaúna river.

### 3.1.2 Outflows and measurements from reservoir operator (SANEPAR)

The Paraná water and waste management company (Companhia de Saneamento do Paraná — SANEPAR) supplied measurements of water level, volume of water withdrawn for treatment, ground outlet discharge, and spillway discharge. The measured water level is shown in Figure 3.6(a) while the discharges are shown in Figure 3.4. However, many inconsistencies were found in the reservoir measurements, so a mass balance was performed with the most reliable measured data.

With the help of the hypsographic curve as well as the water level-volume of the reservoir (Figure 3.5) and measured water level, it is possible to estimate the volume variation of the reservoir. This methodology is used to estimate the mass balance of the reservoir, in order to verify inconsistencies in the discharge measurements before setting up the models.

[1] The total available volume of the reservoir is $48 \times 10^6$ $m^3$ and the outgoing discharge can be estimated by 2.5 $m^3$ $s^{-1}$.

[2] `http://www.mudak-wrm.kit.edu/`

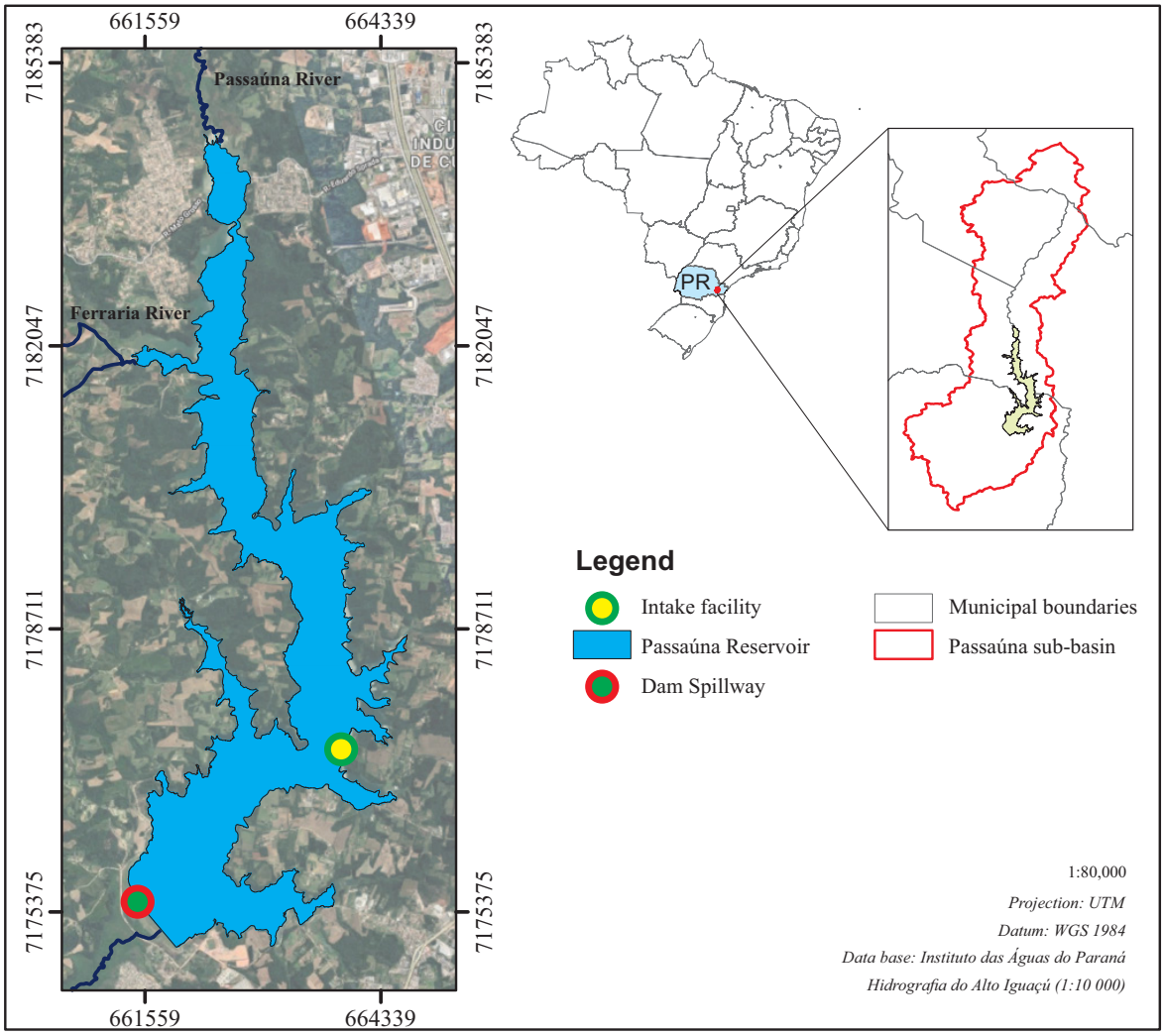


Figura 3.1: Location of Passaúna reservoir in Curitiba, Paraná - Brazil.

### 3.1.3 Meteorological data

Meteorological data was measured by a TECPAR[3] (Instituto de Tecnologia do Paraná) station, as shown in Figure 3.7, for 2018. Data gaps were filled with data collected immediately before the gaps in order to avoid using linear or mean interpolations, as this would be a very simplistic approach. The objective was to simulate the daily variation of the environmental variables.

TECPAR data did not have information about the dew point temperature needed for the CE-QUAL-W2 simulations, thus it was calculated by

$$T_{\text{dew}} = \frac{c\gamma(RH,T)}{b-\gamma(RH,T)}, \tag{3.1}$$

in which

$$\gamma(RH,T) = \ln\left\{RH\exp\left[\left(b-\frac{T}{d}\right)\left(\frac{T}{c+T}\right)\right]\right\}, \tag{3.2}$$

where $RH$ is the relative humidity (%), $T$ the air temperature (°C), and $b = 18.678$, $c = 257.14\,°\text{C}$ and $d = 234.5\,°\text{C}$.

[3]Technology Institute of Paraná

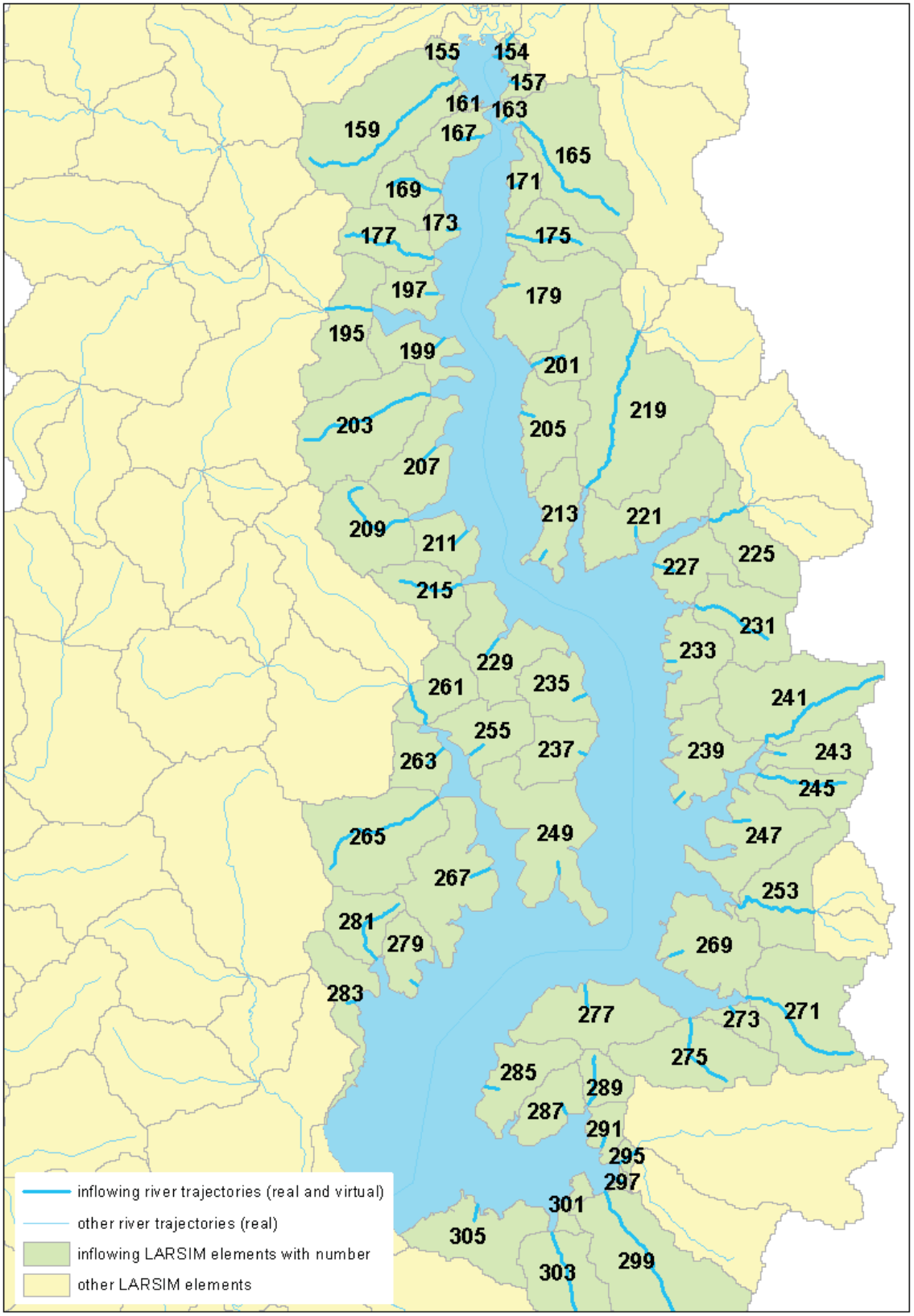


Figura 3.2: Passauna reservoir tributaries location.

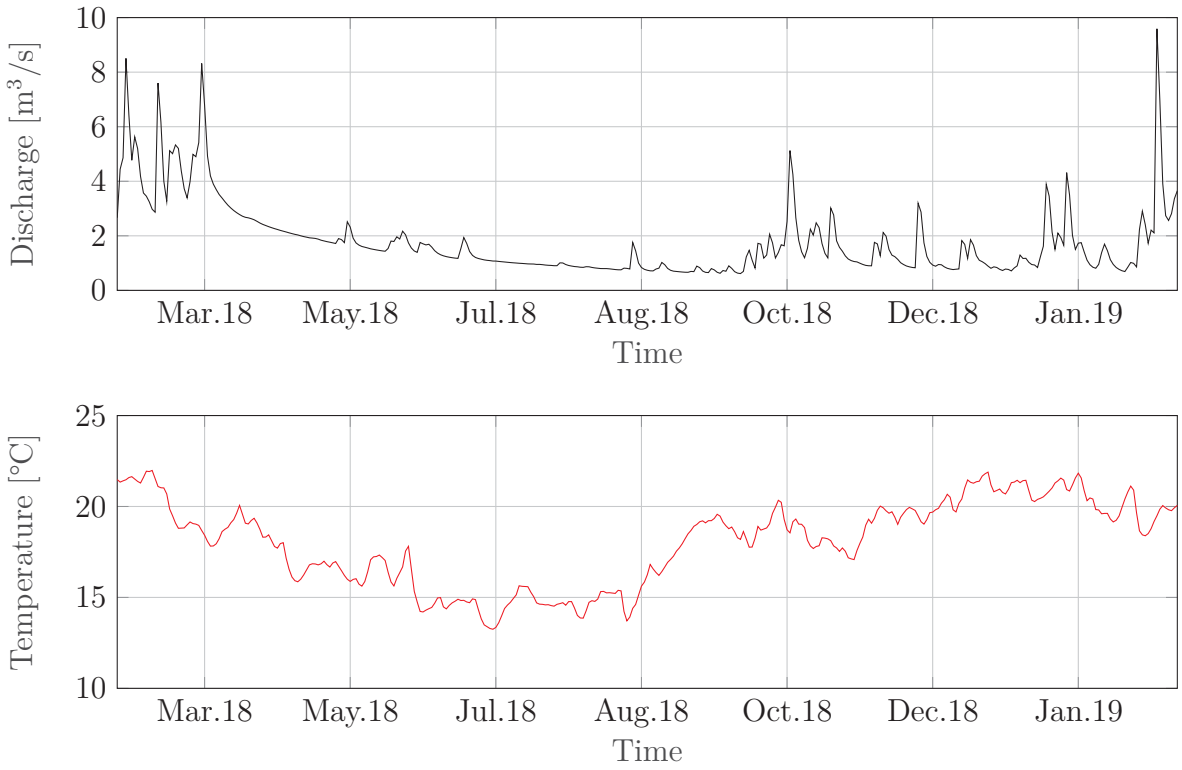


Figura 3.3: Discharge and stream temperature simulated by HYDRON using LARSIM software.

### 3.1.4 Measurement campaigns

Several measurement campaigns were conducted between 2018 and 2019 by UFPR and project partners. Figure 3.8 shows the site of some of the measured data. Temperature measurements were made with the help of ABT Equipment (fixed depth, temporal series), Sontek CastAway CTD sensors (Conductivity, Temperature, and Depth; vertical profiles, snapshot measurement) and a thermistor chain located next to the intake facility. ADCP discharge and velocity measurements were also made, and several other optical sensors were used with distinct purposes.

## 3.2 DATA PRE-PROCESSING AND WATER BALANCE

A time window that allowed a warm-up period for the models was selected, which also matched the time frames on which field measurements of temperature were available. Thus, the time window was defined beginning in 01/03/2018 and ending on 28/02/2019.

Water balance was conducted in order to verify problems with the discharge measurements. A control volume was created around the reservoir and the equation

$$\frac{\mathrm{d}V}{\mathrm{d}t} = \text{out} - \text{in}, \tag{3.3}$$

was integrated over a interval $\Delta t$, to obtain

$$\frac{V_{i+1} - V_i}{\Delta t} = \text{out} - \text{in}. \tag{3.4}$$

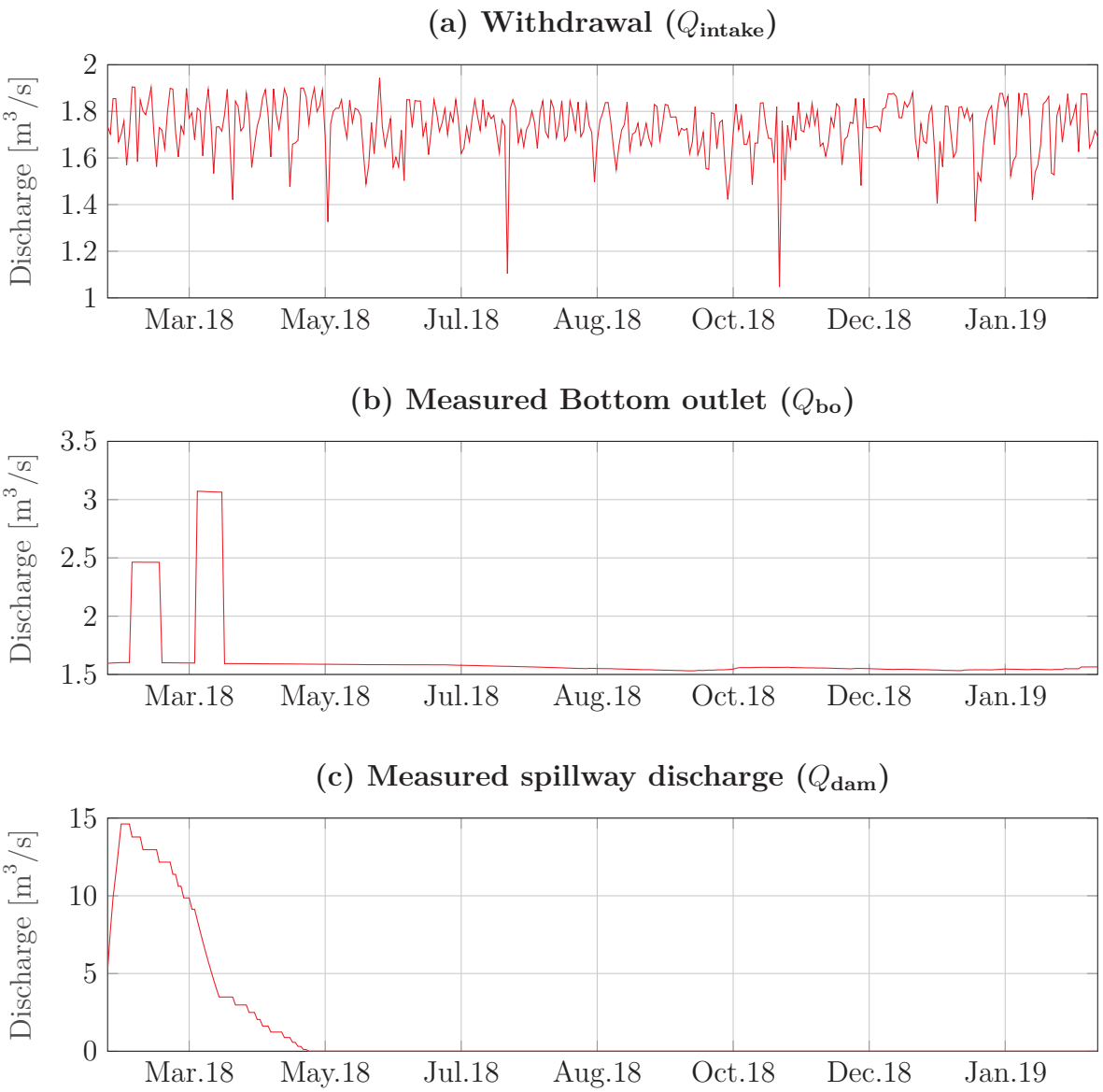


Figura 3.4: Outflows measured by reservoir operator (SANEPAR).

The term "out" represents all the discharges leaving the reservoir, namely, $Q_{\text{intake}}, Q_{\text{bo}}$ and $Q_{\text{dam}}$, and "in" represents all the 64 inflows.

Three scenarios were considered: the first was the simulation of a new bottom outlet discharge using

$$Q_{\text{bo}} = \frac{V_{i+1} - V_i}{\Delta t} + Q_{\text{inflow}} - Q_{\text{intake}} - Q_{\text{dam}}. \tag{3.5}$$

This was possible since the right side of the equation is known or calculated by the water level-volume curve. We made this calculation because field measurements downstream of the reservoir show that the bottom outlet discharge values are overestimated.

The second scenario created a new series for the bottom outlet and the dam discharges using

$$Q_{\text{bo}} + Q_{\text{dam}} = \frac{V_{i+1} - V_i}{\Delta t} + Q_{\text{inflow}} - Q_{\text{intake}}. \tag{3.6}$$

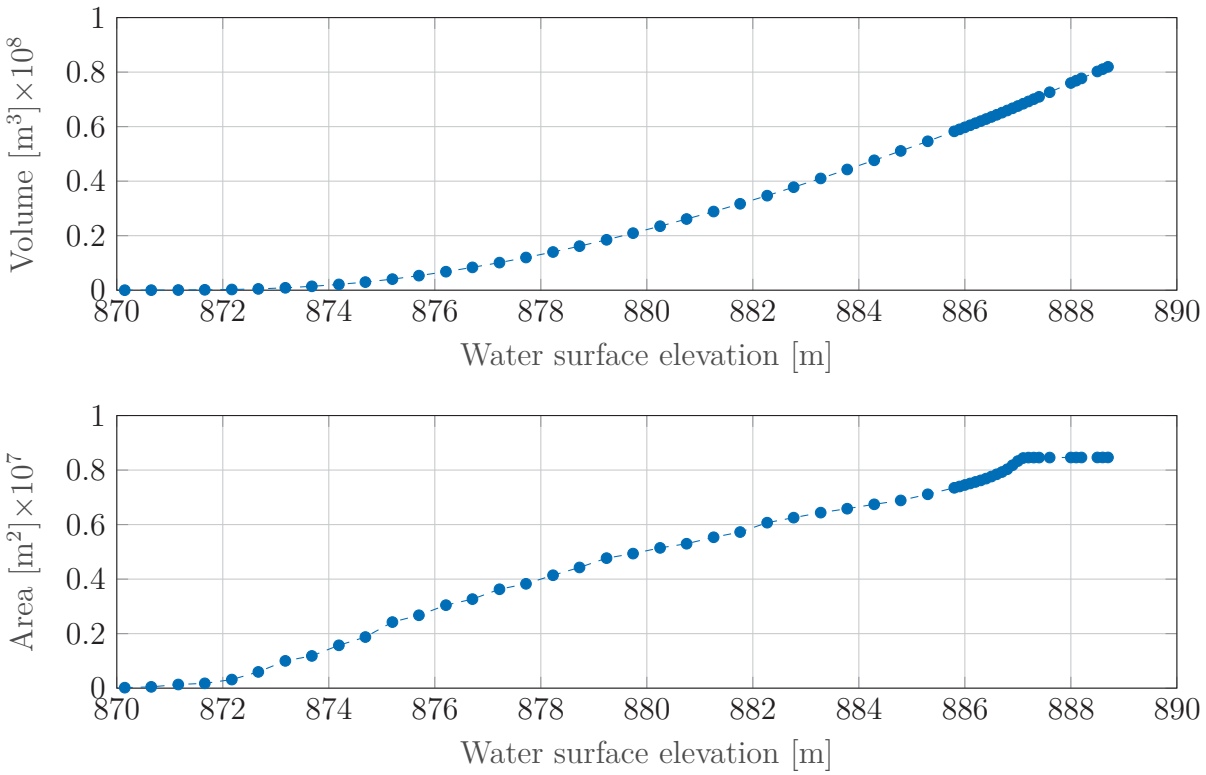


Figura 3.5: Water level-area hypsographic curve and Water level-volume curve.

The reason behind this scenario is that the discharge shown in Figure 3.4 is calculated by an equation that was never calibrated and still uses a standard coefficient in the calculations. And the third scenario created a completely artificial time series for the discharges of the reservoir using

$$Q_{\text{bo}} + Q_{\text{dam}} + Q_{\text{intake}} = \frac{V_{i+1} - V_i}{\Delta t} + Q_{\text{inflow}}. \tag{3.7}$$

This scenario uses only the most reliable data available, which are the water levels measured at the dam and the data from rainfall-runoff models. These artificial time series were used as boundary conditions for the CE-QUAL-W2 model to verify the water balance of the reservoir.

After these calculations, it is possible to further adjust the discharge time series by multiplying the synthetic series created by some $\alpha$ coefficient to generate a time series more faithful to the actual water levels in the reservoir.

## 3.3 ADJUSTMENT OF THE 3D MODELING SUITE: DELFT3D

The first configuration of the three-dimensional model was made with a coarse grid and then shared with the project partners who continued to work and improve the model's attributes. After some tests of the computational grids and adjustments of the boundary conditions, the current configuration was defined.

The discharge inputs used as boundary conditions for Delft3D were: the LARSIM simulations results, measurements of water level at the spillway provided by SANEPAR and the meteorological data from TECPAR. Initially, the data was selected according to the desired time window of the simulation. Table 3.1 shows the initial parameters used to setup Delft3D and other important components to consider.

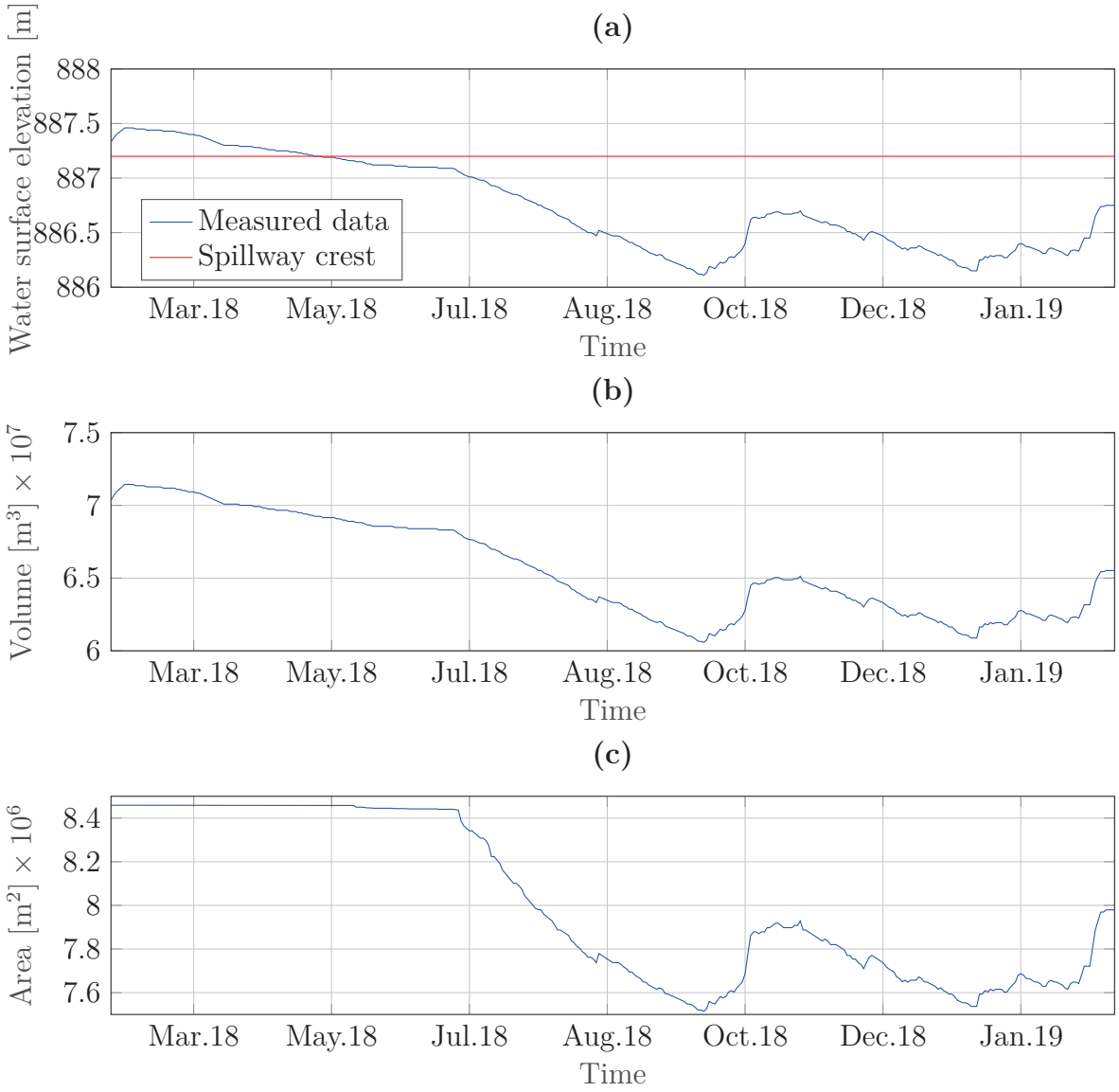


Figura 3.6: Measured and calculated data: (a) Sanepars' water level measurement, (b) volume of the reservoir and (c) area of the reservoir.

Figure 3.9(a) and 3.9(b) shows the bathymetry, coarse grid and location of the tributaries provided by LARSIM simulations.

## 3.4 ADJUSTMENT OF THE 2D MODELING SUITE: CE-QUAL-W2

The set up of the two-dimensional model was extremely complicated (compared to the 3D model) and laborious with several time-consuming steps. Various configurations, options, and tools were tested until the current solution was found. The main problem was in the construction of the file with bathymetric data. Even after the construction of these files, the model had to go through several sections of bug fixing and adjustments regarding data compatibility and adequacy.

The bathymetry file of the reservoir used in CE-QUAL-W2 was created using the open-source geographic information system software QGIS (Figures 3.9(c), 3.10(a)

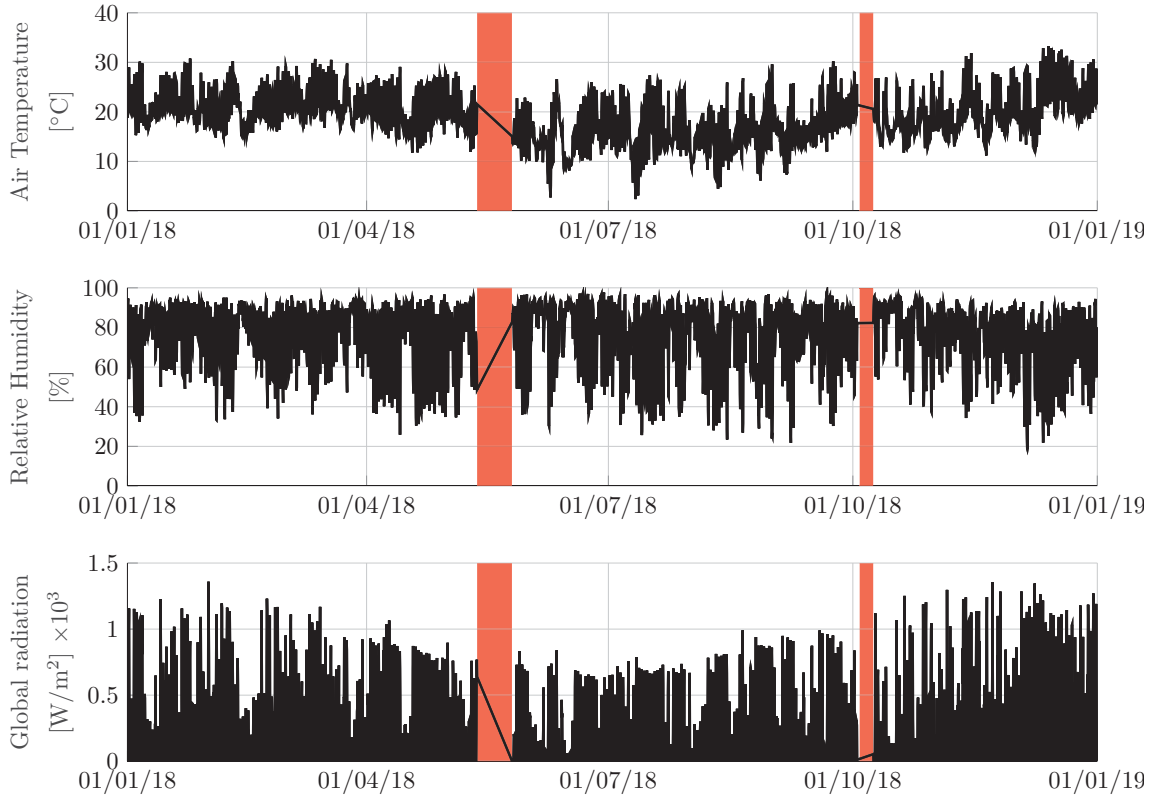


Figura 3.7: Samples of the measured data by the TECPAR station and data gaps identification for the year 2018.

Tabela 3.1: Initial parameters, models and system utilized initially in Delft3D

| Parameter | Value or option selected |
|---|---|
| Num. of layers | 20 |
| $\Delta t$ | 0.1 min |
| Turbulence model | $k-\epsilon$ |
| Heat flux model | Ocean |
| Coordinate system | $z$ |
| Grid | Curvilinear |

and 3.10(b)), with the plug-in "CE-QUAL-W2 Bathymetry"[4] being essential in this task. After a few format suitability tests, the boundary conditions were adjusted in the needed way and used as input for the model. The time frame selected for CE-QUAL-W2 was the same as that selected for Delft3D simulations.

The grid for the CE-QUAL-W2 contains 20 layers ($z$ direction, Figure 3.10(b)), 2 branches ($xy$ plane, Figure 3.9(c)) and 82 segments divided among the two branches ($xz$ plane, Figure 3.10(b)). The minimum time step used was 0.1 min, but the model can increase the time step accordingly if the results are not affected by this change. Table 3.2 shows the initial parameters used to setup CE-QUAL-W2 and other important components to consider.

[4] https://plugins.qgis.org/plugins/create_bathymetry/

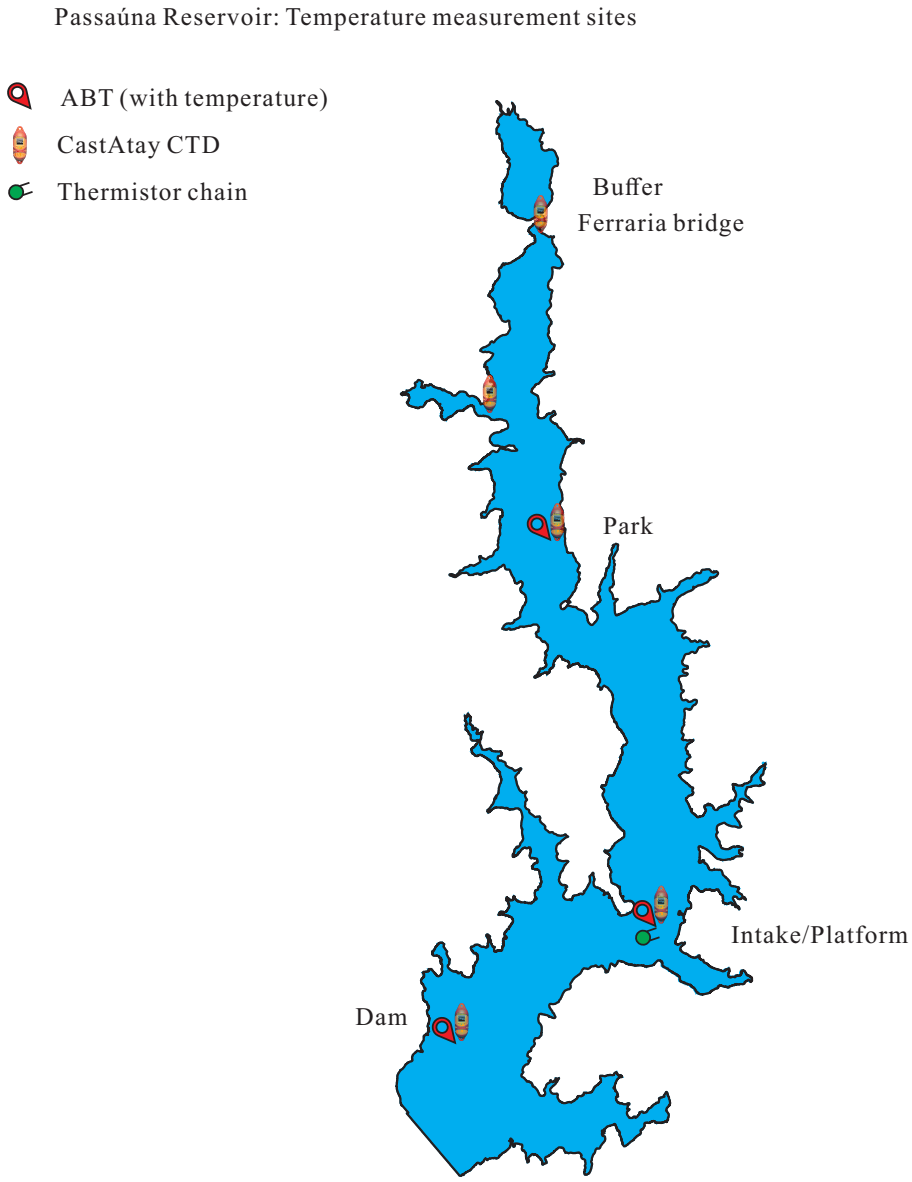


Figura 3.8: Location of measured data along the reservoir.

Tabela 3.2: Prameters, models and system utilized in CE-QUAL-W2

| Parameter | Value or option selected |
|---|---|
| Num. of layers | 20 |
| Num. of segments | 80 |
| Num. of branches | 2 |
| Grid spacing ($\Delta x$) | Approx. 140 m |
| Turbulence model | W2 |
| Horizontal eddy viscosity | 0.0926 $m^2$ $s^{-1}$ |
| Horizontal eddy diffusivity | 0.0926 $m^2$ $s^{-1}$ |

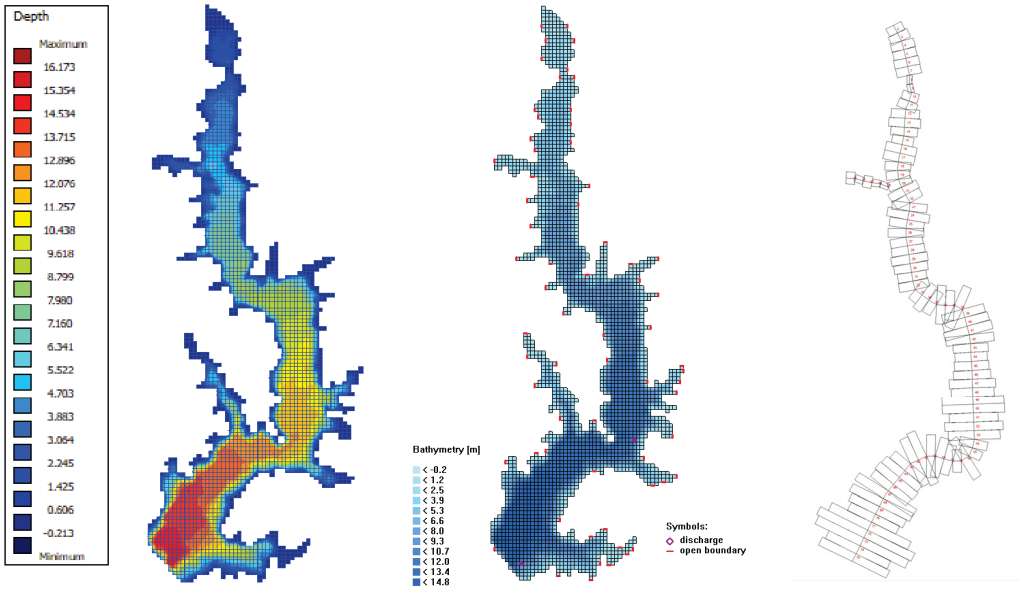


(a) (b) (c)

Figura 3.9: Passaúna reservoir: (a) grid and bathymetry in Delft3D. (b) grid and location of open boundaries — tributaries location — in Delft3D. (c) Plain view (segments data) of the bathymetry in CE-QUAL-W2.

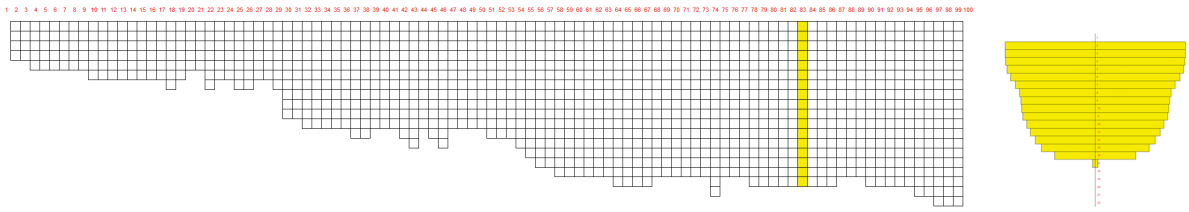

(a) (b)

Figura 3.10: Passaúna reservoir: (a) grid in the plane $xz$: Layers and Segments. (b) grid in the plane $xy$: Layers

## 3.5 CRITERIA OF COMPARISION AND EVALUATION

The results were compared with field data using Root Mean Square Error ($E$) defined by

$$E = \left[\frac{1}{n}\sum_{i=1}^{n}(x_{\text{obs},i} - x_{\text{mod},i})^2\right]^{1/2}, \tag{3.8}$$

in which $n$ is the number of observations, $x_{\text{obs},i}$ the measured data and $x_{\text{mod},i}$ is the model results data. This measure is always a positive number and a low value of $E$ indicates better results.

The standard deviation $\sigma$, as a measure for the variation of the data set calculated by

$$\sigma = \left[\frac{1}{n-1}\sum_{i=1}^{n}(x_i - \overline{x})^2\right]^{1/2}, \tag{3.9}$$

was also used on the analysis. Whenever possible, the Pearson correlation coefficient was also used as a measure of linear correlation between two data sets, calculated by

$$r = \frac{1}{n-1}\sum_{i=1}^{n}\left(\frac{x_{\text{obs},i} - \overline{x_{\text{obs},i}}}{\sigma_{\text{obs}}}\right)\left(\frac{x_{\text{mod},i} - \overline{x_{\text{mod},i}}}{\sigma_{\text{mod}}}\right), \tag{3.10}$$

in which $\sigma$ denotes the standard deviation of the data.

Instead of showing the values of the metrics above, the Taylor diagram will be presented whenever possible, which was specifically built to indicate which of the models best represents a data set. This diagram was first introduced by Taylor (2001) and it summarizes the Root Mean Square, Pearson Coefficient and standard deviation in one diagram. These three statistics are related by

$$E^2 = \sigma_r^2 + \sigma_s^2 - 2\sigma_r\sigma_s r, \tag{3.11}$$

in which $\sigma_r$ is the standard deviation of the observed data and $\sigma_s$ is the standard deviation of the simulated field.

Figure 3.11 shows an example of a Taylor Diagram with four points: the $x$-axis shows the reference value; the $y$-axis shows, radially, the standard deviation of the modeled data, which is $\sigma_A = 0.5$, $\sigma_B = 1$ and $\sigma_C = 1.25$; the angle between the $x$ and $y$ axis shows the Pearson correlation coefficient, which is $r_A = 0.95$, $r_B = 0.75$ and $r_C = 0.25$; and the centered Root Mean Square is shown by the green lines coming off of the reference dot, which are $E_A \approx 0.5$, $E_B \approx 0.7$ and $E_C \approx 1.4$.

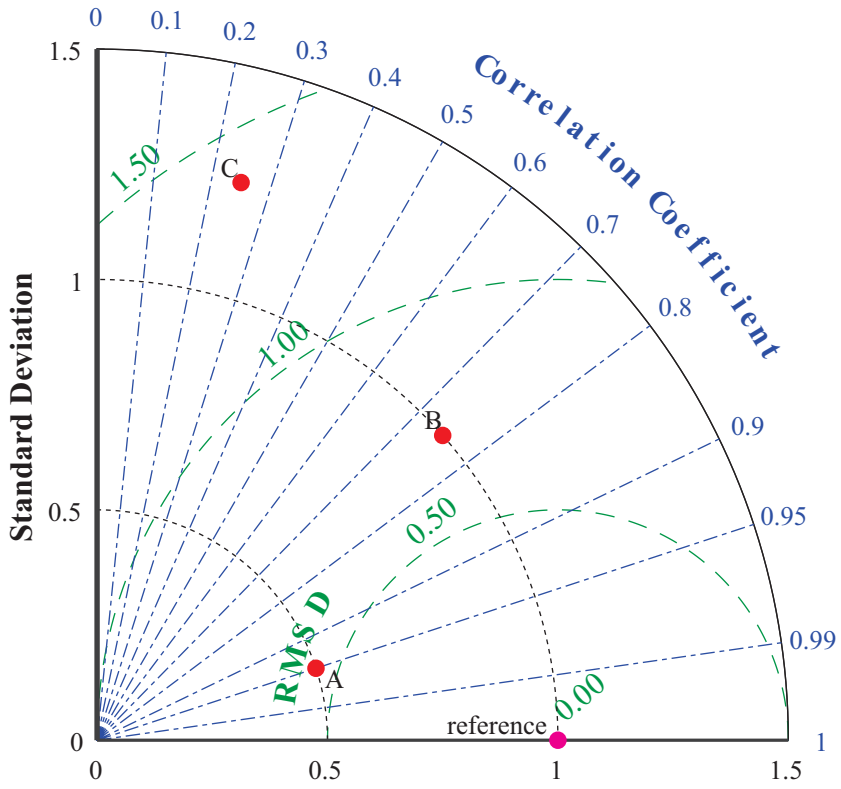


Figura 3.11: Example of a Taylor Diagram.

Other statistical parameters, such as boxplots and mean values for profiles were computed. The evaluation of the height of the thermocline, the time needed to run the simulations, the performance, stability, and easiness to set up and get information from the model were also taken into account.

# 4 RESULTS AND DISCUSSION

The results are structured as follows: initially, the results for the reservoir mass balance are presented. Next, the results obtained by the two-dimensional model are presented, and then the results obtained by the three-dimensional model. Finally, a discussion of the main results is presented.

## 4.1 WATER BALANCE AND WATER LEVEL FOR CE-QUAL-W2

From the measured water level variation (Figure 3.6) and the water level-volume curve (Figure 3.5), along with equations (3.5), (3.6) and (3.7) and daily measurements of the outflows (($Q_{\text{intake}}, Q_{\text{bo}}$ e $Q_{\text{dam}}$) and inflows ($Q_{\text{inflow}}$), the artificial series for the reservoir output was calculated. This artificial series were entered in the CE-QUAL-W2 model and the behavior of the level was studied. The best result for this analysis is presented in Figure 4.1.

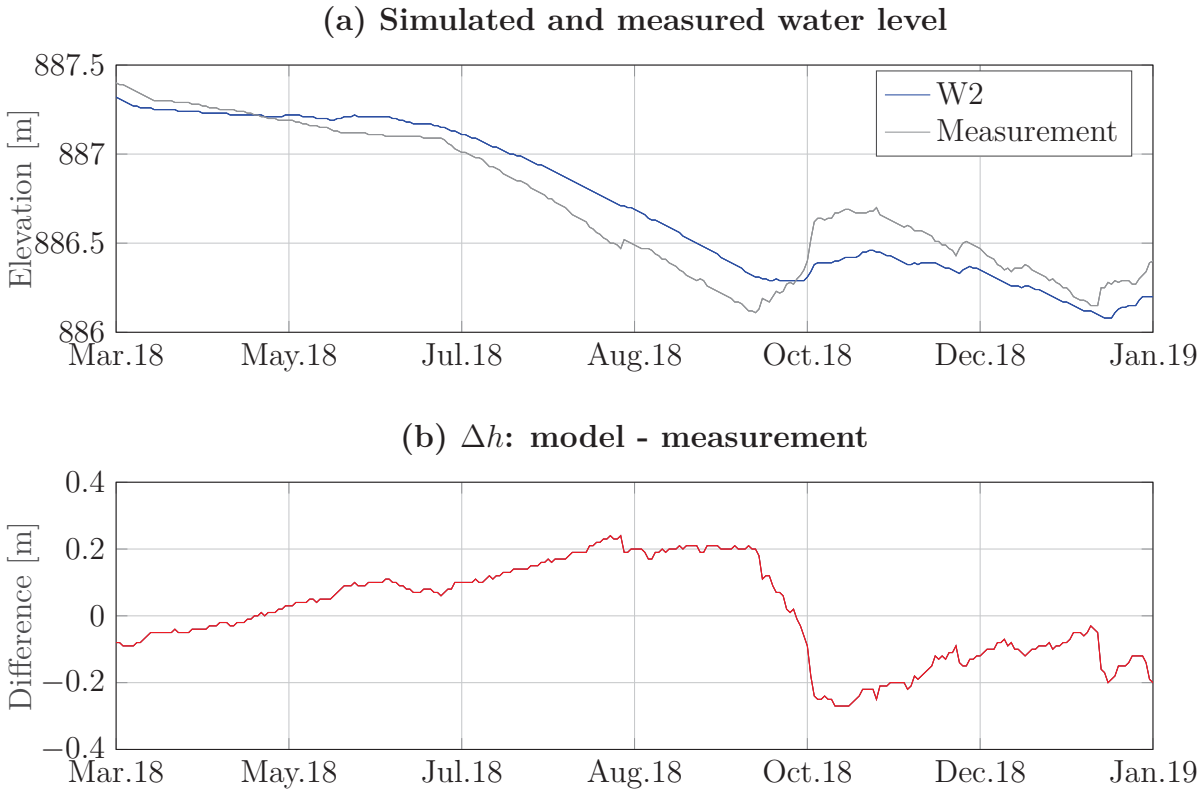


Figura 4.1: Comparison between measured (Sanepar) and simulated (CE-QUAL-W2) water level.

By using only the data measured by SANEPAR, the results for the water level were judged inadequate as the model produced a maximum error of 45 cm. The artificial series for the produced output was also judged inadequate as it returned even worse results than those of the previous case, so the flow series was gradually reduced until it produced a satisfactory result. The maximum errors of this analysis are presented in Table 4.1.

This completely artificial output series reinforces the hypothesis that the measurements for the reservoir outputs may be incorrect, if we take the water level of reservoir

Tabela 4.1: Results for the maximum water level error according to the used discharge output series.

| Setting | Maximum error value | % reservoir depth |
|---|---|---|
| Sanepar measurement | 0.45 m | 2.50 |
| $Q_{out} = Q_{intake} + Q_{bo} + Q_{dam}$ | 0.51 m | 2.83 |
| $Q_{out} = \alpha \times (Q_{intake} + Q_{bo} + Q_{dam})$, $\alpha = 0.91$ | 0.27 m | 1.50 |

to be true. The need to adjust the same series by coefficients may indicate that daily values for inflows and outflows are probably not sufficient to characterize the reservoir. The energy balances are also expected to be limited by the quality of the input data of the models.

## 4.2 CE-QUAL-W2 RESULTS

First, the results of the CE-QUAL-W2 model are presented followed by a brief analysis.

### 4.2.1 Hydrodynamics

Based on ADCP measurements, a verification of simulated velocity data was performed. Figure 4.2 shows the velocity data between October 30, 2018 and December 10, 2018. From the available data, the statistics for 3, 5 and 8 m of depth was calculated in order to follow how the reservoir hydrodynamics behaved in the models. Generated velocity profiles were not compared as it would not be fair to compare specific measurements (such as ADCP measurements) with average temporal and spatial data generated by the models: the objective is to verify if the tendency is being followed and not if the models are able to reproduce the measurements perfectly.

It is worth noting that the W2 model obtained good average results for the velocities in the deep parts of the reservoir, but with a greater variation than that presented by the ADCP data. The statistics generated for the shallow part of the reservoir (approximately 3 m deep) showed that the water flows in the opposite direction to that presented by the measurements. This may indicate that the CE-QUAL-W2 model is more sensitive to changes in the wind direction, which is the main hydrodynamic force in this region, or that the drag coefficient is too high. From the time series of velocities (Figure 4.2(c)), the 2D model seems to be able, at some moments, to adjust part of the phase as well as the amplitude of the waves.

It is worth remembering that the reservoir simulated presents extremely low current speeds and the main hydrodynamic forces are inflows and wind speed and direction. The simulated velocities for the whole extension of the reservoir, which are shown in Figure 4.16(b), are very low. Thus, the results are in agreement as the models did not foresee any inconsistent results.

### 4.2.2 Temperature

#### *4.2.2.1 Time series of temperature*

Figure 4.3 shows the results obtained by the models and ABT measurements for the chosen observation points, with subfigures (a) and (b) showing the data referring to the capture point. The model CE-QUAL-W2 was able to adequately simulate the temperature

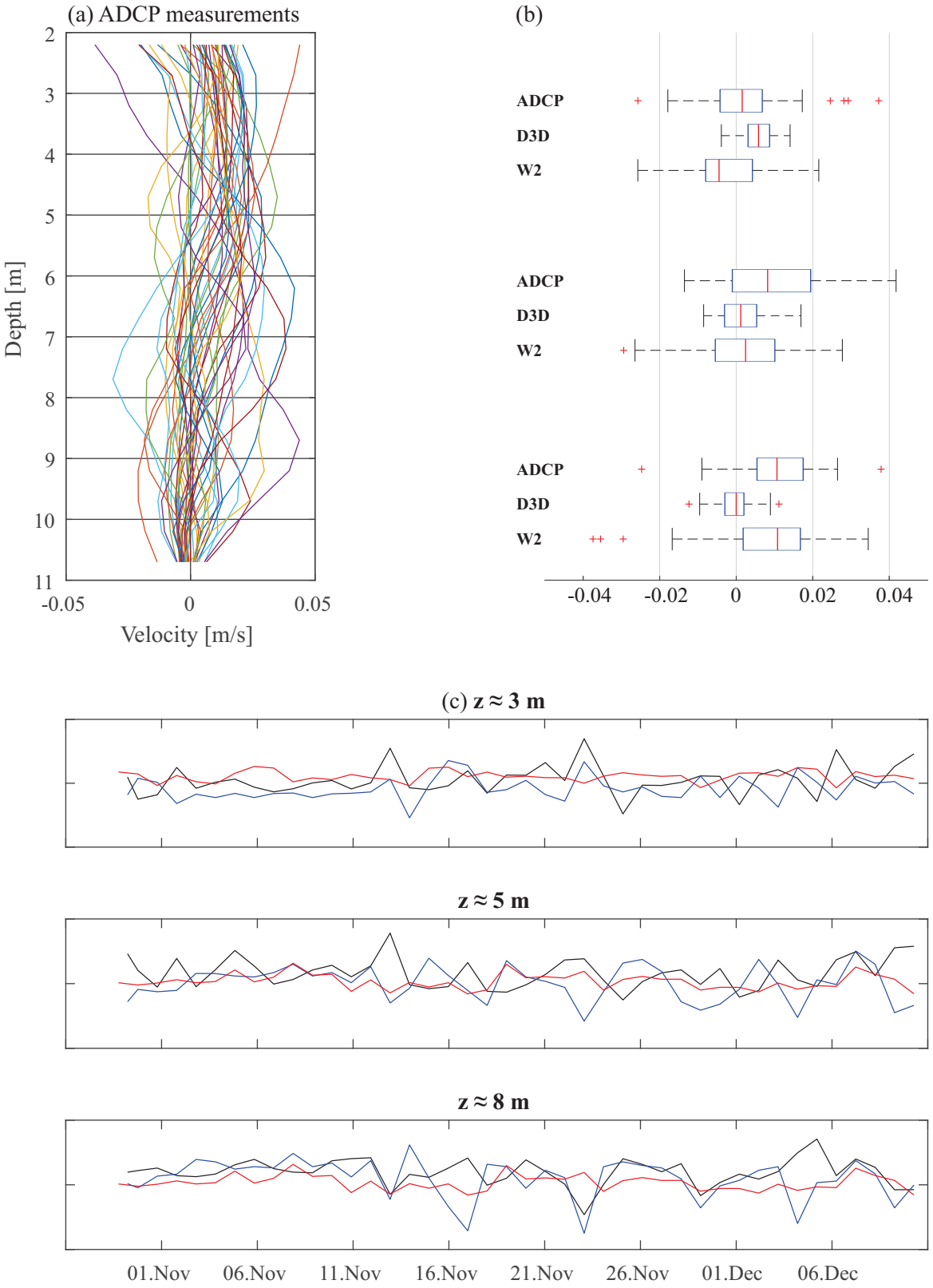


Figura 4.2: The horizontal velocity of the water for the intake. (a) ADCP measurements from 30th October 2018 until 10th December 2018. (b) Boxplots for the time series of 3, 5 and 8 m deep respectively. (c) Time series of the horizontal water velocity; ADCP measurements in black, CE-QUAL-W2 simulated values in blue and the Delft3D simulated values in red.

Tabela 4.2: Errors of the temperature time series obtained by the models to those measured by ABT.

| | Intake | | Park | | Dam | |
|---|---|---|---|---|---|---|
| | CW2 | D3D | CW2 | D3D | CW2 | D3D |
| Average value | 0.515 | 1.874 | −0.255 | −0.735 | −1.782 | −1.619 |
| Highest value | 3.374 | 5.988 | 1.373 | 1.974 | 3.050 | 3.258 |

variations of the period under analysis and was able to adjust the phases of oscillations as well as the wave amplitudes. However, the model almost always underestimated the temperature value (maybe because of the chosen sediment temperature used — 15 °C), except in May 2018 when the model presented a strange behavior, simulating a heating of the water that was not captured by the local sensor. This happened because of the chosen method for the filling of the data gaps of the meteorological data. The greatest error in the temperature value was of 3.4 °C.

The results for the Park's observation point are shown in Figure 4.3(c) and (d). The model was able to correctly simulate the temperature variations for this period, even though the available measurements for this observation point are scarce. On average, the simulated temperatures exceed those observed by the sensor, with a more discrete variation than the previous case in which the greatest difference between the measured and the simulated temperatures was around 1.4 °C.

Figures 4.3(e) and (f) show the results obtained by the models and ABT measurements in the dam region. It should be noted that the measurements available for this observation point have long failures and that the model could not simulate well the temperature variations of the period. At this point, the model overestimated the temperature value by a maximum of 3 °C and made a lot of mistakes in the temperature distribution, with the proximity to the computational grid limits as a potential source of this discrepancy. Another possibility is that the measurement was flawed since both models produced similar results for this point.

Table 4.2 shows the values of the maximum and mean errors of the simulated and measured temperature time series by ABT, for the Delft3D and CE-QUAL-W2 models. Figure 4.4 shows the Taylor diagram for the time series presented in Figures 4.3.

It is possible to observe, in Figure 4.4, a good adherence among the simulated values for the captured region, where the correlation coefficient between the series for this point exceeded 95% and the two series had almost identical standard deviations. For the Park point, the good statistics were repeated with a correlation coefficient of approximately 90% and a standard deviation slightly higher than that presented by the measured series. For the dam results, the tendency was reversed and the statistics got much worse: the modeled values were much more varied than those measured and the correlation coefficient indicates a very weak correspondence.

For the captured region, in addition to the measurements made by ABTs, measurements through thermistor currents were also performed. Figure 4.5 shows the time series measured by this current for the depths of 2, 4, 6, 8 and 10 m.

Figure 4.6 shows the comparison between the temperatures simulated by CE-QUAL-W2 and those measured by the thermistor currents at correlated depths. It is worth noting that, for the surface region, the correspondence between the time series is stronger than that presented for the bottom of the reservoir. Thus, while the model is able to capture well the surface variations, it tends to overestimate the temperature at the

bottom of the water body. Again, the CE-QUAL-W2 model presented a heating of the water column in May 2018, which was not observed by the thermistors. It is possible that the simulated temperature of one of the 62 tributaries of the reservoir is influencing these results.

The diagram in Figura 4.7 shows that the statistics for time series get worse as temperature values for deeper region are analyzed. The statistics for the depths of 2 and 4 m are practically identical: they show a standard deviation close to that of the thermistors and a correlation coefficient higher than 95%. The same is repeated for the statistics for depths of 6 and 8 m. The statistics of the time series for the depth of approximately 10 m worsened significantly.

The contour graphics for the measured and simulated temperatures for the captured point are shown in Figures 4.8. A good correspondence between measurements and models can be easily observed through these graphs.

#### *4.2.2.2 Temperature Profiles*

The comparison between the temperature profiles simulated by the models against those produced by CTD measurements is presented below. Figure 4.9 shows the profiles measured (gray line) and the profiles simulated by the CE-QUAL-W2 model (blue line). The statistics for the temperature profiles are shown in Figura 4.10. There is a wide variation in the results by CE-QUAL-W2.

The model mixed the reservoir more, as also verified by Figures 4.11 and 4.8 In order to better represent the amplitudes of these values, additional adjustments must be made to the configurations of the two-dimensional model.

#### *4.2.2.3 Thermal Stratification*

From the model results it is possible to estimate for how many days the reservoir is thermally stratified and the degree of this stratification. Figures 4.11 shows the simulated behavior for the surface and the bottom temperatures of the reservoir as well as the difference between them for the Bridge, Park and Intake measurement points. It is worth remembering that, for the captured region, the CE-QUAL-W2 model overestimated the bottom temperature of the reservoir for the period under analysis.

Table 4.3 shows the number of days that the reservoir presented thermal stratification according to data from the thermistors and the results of CE-QUAL-W2 simulations. The previous result is repeated showing that CE-QUAL-W2 mixes the properties of the reservoir very quickly so the reservoir remains uniform for most of the time.

The thermistors observed that the reservoir had a gradient of temperature greater than 3 units of degree for 34% of the time of the studied period. The simulation of the reservoir with the CE-QUAL-W2 model shows that the reservoir had gradients with the same order of magnitude for only 3% of the studied period. Only for milder stratifications is the result more satisfactory.

The higher speed in which the CE-QUAL-W2 model mixes the reservoir can be explained by the physical shape of the reservoir and the way the model handles bathymetry. As shown in Figure 3.5, the reservoir has a very linear variation between quota, volume, and area and, as shown in Figure 3.10(a), cells of equal size are gradually added vertically to the computational grid. This gradual addition along with the absence of transverse variations fosters the faster mixing of properties.

Tabela 4.3: The number of days the reservoir is thermally stratified in the water intake region.

| | Measured (Thermistors) | Simulated (CE-QUAL-W2) | Simulated (Delft3D) |
|---|---|---|---|
| $2 < \Delta T \leqslant 3$ | 117 | 13 | 88 |
| $1 < \Delta T \leqslant 2$ | 50 | 33 | 48 |
| $\Delta T \geqslant 1$ | 85 | 98 | 81 |
| $\Delta T < 1$ | 90 | 198 | 125 |

Tabela 4.4: The number of days the reservoir is thermally stratified in the park and bridge region.

| | Bridge | | Park | |
|---|---|---|---|---|
| | CE-QUAL-W2 | Delft3D | CE-QUAL-W2 | Delft3D |
| $2 < \Delta T \leqslant 3$ | 0 | 4 | 0 | 1 |
| $1 < \Delta T \leqslant 2$ | 4 | 64 | 21 | 8 |
| $\Delta T \geqslant 1$ | 36 | 164 | 40 | 85 |
| $\Delta T < 1$ | 324 | 132 | 303 | 270 |

## 4.3 DELFT3D RESULTS

Now the main results obtained by the three-dimensional model are presented.

### 4.3.1 Hydrodynamcs

As shown in Figure 4.2, the 3D model produced slightly worse results for hydrodynamics in the captured region. This model predicts much lower velocities for the deep parts of the reservoir and, at several times, predominant velocities in the opposite direction observed by ADCP. In general, Delft3D results are much less varied than those presented by measurements or by the 2D model. In Figure 4.16(a), we notice that these slightly worse results do not make much difference to the movement of water. The velocities in the reservoir are always very low, with expressive values only in the constriction generated by the bridge in the buffer region. The results do not vary much for the interior of the reservoir.

### 4.3.2 Temperature

#### *4.3.2.1 Time series of temperature*

Back to Figure 4.3, it is observed that the Delft3D model is able to simulate well the temperature variations of the analyzed period but, similarly to the CE-QUAL-W2 model, it almost always underestimates the temperature values. The most critical errors are found in the heating period of the air temperature between October and December, when the water temperature increases in a uniform way but the model simulates this change in a slower way. For this period, the model produces the greatest difference in the temperature values, underestimating the values in about 6 °C.

For the Park region, the behavior of the two models was similar: both models slightly overestimated the temperature value but Delft3D presented more abrupt variations in its results.

For the dam region, the models tended not to be able to properly simulate the thermal balance. The Delft3D model shows slightly better results than the CE-QUAL-W2

Tabela 4.5: Non-normalized data for Root-Mean-Square-Error for the water intake region. Data comparing simulated values and those observed by the thermistors chain.

| Location | CE-QUAL-W2 | Delft-3D |
|---|---|---|
| Surface | 0.9315 | 0.4646 |
| Bottom | 1.2872 | 0.6067 |

but still shows poor results, which reinforces the possibility that the measurements are incorrect.

From the statistics presented in Figuras 4.4 and 4.7, a greater variation in the results by the CE-QUAL-W2 model can be seen. This shows that the 3D model is producing more accurate results than the 2D model, indicating that transversal variations in properties somehow alter the balance of properties in the Passaúna reservoir. Even though, the results of both models can be considered excellent. The accuracy of the 2D model results is limited by the absence of transversal balance, but the quality loss is not excessive and the computational cost is extremely lower.

The data presented in Figure 1 are normalized for better use of the Taylor diagram, thus, Table 2 presents the results for the Root-Mean-Square-Error metric without normalization. We have, therefore, that the Delft3D model proves to be much more accurate and precise than the CE-QUAL-W2 model.

#### *4.3.2.2 Temperature profiles*

Based on Figures 4.9 and Figure 4.10, a good match between model and measurement can be observed. In general, the 3D model obtained more accurate results than the 2D model, even with the difference between the bathymetries and grids at the point of capture. Figure 4.9 shows that the depths simulated by the 2D model are much more similar to those obtained by CTD measurements.

Figure 4.14 shows why this discrepancy occurred: the 3D model has fewer computational cells in the capture region (near the left margin of the figure) but the existence of cells in the transversal area compensates the results and the model produces good statistical coefficients.

#### *4.3.2.3 Thermal Stratification*

Based on Table 4.3, the 3D model simulated a thermal stratification above 3 °C for the capture region for 26% of the time. This value is consistent with measurements by thermistor chain. As shown in Figures 4.13(c), there are times when the temperature difference reaches 6°C, with such a level of stratification also appearing in thermistor measurements.

The 3D model also predicted, for the Bridge and Park points, a greater thermal stratification than the 2D model. As shown in Table 4.4, the temperature difference was less than 1°C for 89% of the time for the 2D model in the bridge region, while the 3D model simulated the same degree of stratification for only 36% of the time. For the Park region, the 3D model simulated a well mixed reservoir with temperatures above 1 °C for only 2% of the time.

Tabela 4.6: Data regarding the time required for processing and the volume of data generated by the models.

| Model | Simulation Time | | Volume of data |
|---|---|---|---|
| D3D | $z$-system | 6d 10hrs | 52.6 Gb |
| | $\sigma$-system | c. 17d 7hrs | |
| W2 | | 1 min 20s | 50 Mb |

## 4.4 SIMULATION TIME

Table 4.6 shows that the 3D model using the $z$-coordinate system requires 9.000 times more processing time than the 2D model, and generates a data volume 4 orders of magnitude higher. The results are even worse when comparing the processing time for the 3D model using the $\sigma$-coordinate system. Both models ran on a computer with an Intel i7-3960X, 3.30 GHz processor with 16 GB of RAM in a 64-bit operational system.

The difference between the times needed for processing is due to the difference between the computational grids and the time integration step used in the simulations: the three-dimensional grid has about 300 thousand cells with the values of all properties being reassessed every 6 seconds in numerical integration, while the two-dimensional grid has only about 1.100 cells that are reassessed every 320 seconds (time step).

## 4.5 DISCUSSION AND COMPARISON

This section presents an integrated comparison of the results obtained by the two models.

### 4.5.1 Boundary conditions

The creation of an artificial series of flows for the two-dimensional model proved to be the most appropriate way to assess the problem as without it the results would be extremely compromised, making it impossible to obtain significant results.

Changes in the water balance are expected when assessing the problem by 2D models, but the changes in hydrodynamics are very small, localized, and often not captured by other regions of the reservoir. During the execution of the models, when exchanging one series of flows for another, changes in the velocity distributions were noticeable only in the region where the boundary condition was located. This change in the velocities was not perceived by the nearby segments.

In order to study the thermal stratification of the reservoir, adjusting the water level proved to be more important than adjusting the velocities. Naturally, if the measurements and boundary conditions were more reliable, the analysis would be more hydrodynamically rigorous. As it was not the case in this study, the closing of the water and thermal balance of the reservoir was conducted in the best possible way using the available data with its own uncertainties.

As the three-dimensional model was forced also by level and used the water level as boundary condition, it presents unique characteristics when assessing the problem. It maintains an open contour in its boundary, that is, the dam, which allows the entrance and exit of water by demand in order to close the water balance and adjust the level. Such option is not available in the two-dimensional model.

The local hydrodynamics of the 3D model is also affected by the way it handles this open boundary. However, for regions far from the contours that present flows, the main hydrodynamic force is the wind. Therefore, a more effective way to improve the results for the velocities profiles in the reservoirs is to obtain data on wind speed and direction with better quality and closer to the studied site. The wind data available for this study, although excellent, are distant from the actual reservoir site by about 3 km, thus applying uncertainties in the entire analysis.

### 4.5.2 Temperatures

Both models are capable of reproducing and simulating the thermal situation of the reservoir. The 2D model produced, on average, more dispersed and less accurate results than the 3D model, but still with excellent results. Even with little effort in changing its calibration coefficients, the 2D model was able to produce similar results to the 3D models with better results at some points. This shows that the presence of another dimension does not necessarily imply better products and only the quality of the data and proper treatment of the parameters can influence the results.

According to the aforementioned results, the numerical method used by CE-QUAL-W2 has a tendency to reduce the numerical diffusion, which contradicts what was shown where the 2D model mixes the reservoir quickly. Besides the bathymetry, it can be said that the eddy viscosity coefficients have very high values, but these coefficients should be lower considering that the numerical method already tries to reduce this diffusion. The comparison between calibration coefficients used by models of different dimensions could not be directly made.

Both models produced poor results for the ABT of the dam and the temperature profile of February 2018. Obviously, mathematical equations and physical laws are obeyed, as well as computational limitations, but the ability of the models to make mistakes in the same proportions for the same data set can be seen as positive because it indicates a good adequacy of both tools.

By analyzing the results of the thermistors, the 3D model showed more efficiency and correlation to the field measurements. However, the 2D model would produce similar or better results if its calibration coefficients were better adjusted, for 2D models are easier to calibrate since they require much less computational effort.

In the way it is built for the Passauna reservoir, the 2D model is capable of producing density currents, or intrusive flows, with the same capacity as the 3D model, as shown in Figure 4.17. However, if any future work aims to study these phenomena, a readjustment of the model bathymetry is recommended. The linear characteristic of the reservoir along with a relatively coarse grid may not favor the simulation of these flows and a more refined grid in the vertical and longitudinal direction is more suitable for the study of these flows.

By analyzing the simulated transversal variations in the intake facility by the 3D model shown in Figures 4.17, we have one of the fundamental results of this study: transversal variations are not relevant for temperature distribution at the intake region. A 2DV model is enough to reproduce the thermal and hydrodynamic stratification of the reservoir.

The coordinate system of the 3D model also influences the results. The chosen coordinate system ($z$-coordinates) is more likely to produce good results for stratification, while the $\sigma$-system tends to more numerically mix the reservoir. Results from the use of

the $\sigma$-system, besides being worse, require much more processing capacity, so the choice of the coordinate system for the 3D model was the ideal one for the study.

### 4.5.3 General aspects

The two-dimensional models, despite using mean values in the transversal sections, are perfectly capable of reproducing and simulating the reservoir conditions, as observed by the results. The results of 2D models, although less accurate than 3D models, show that simplifying the problem is often a feasible solution, as these simplifications avoid the need for complex data acquisition and treatment as well as facilitate the simulation. This naturally lowers the cost of the entire modeling and management process.

As expressed earlier, 2DV models are less explored in literature and, because of that, they lack the tools capable of handling input, output and boundary condition data. For this reason, they are much more difficult to use and their application requires a lot of patience from their users. CE-QUAL-W2 is one of the models that lack tools to treat their data, particularly when creating the bathymetry file and computer grid definition, which are essential for the model to work properly.

The tools for post-processing 2D data are also very scarce, confusing, and often disappointing, with it sometimes making the processing of results arduous, requiring the development of new codes and tools every time someone tries to run the model from the beginning. Such difficulties are not present in three-dimensional models and, although the volume of data generated by 3D models is much greater than that generated by 2D models, it is much easier to work with the results of three-dimensional models.

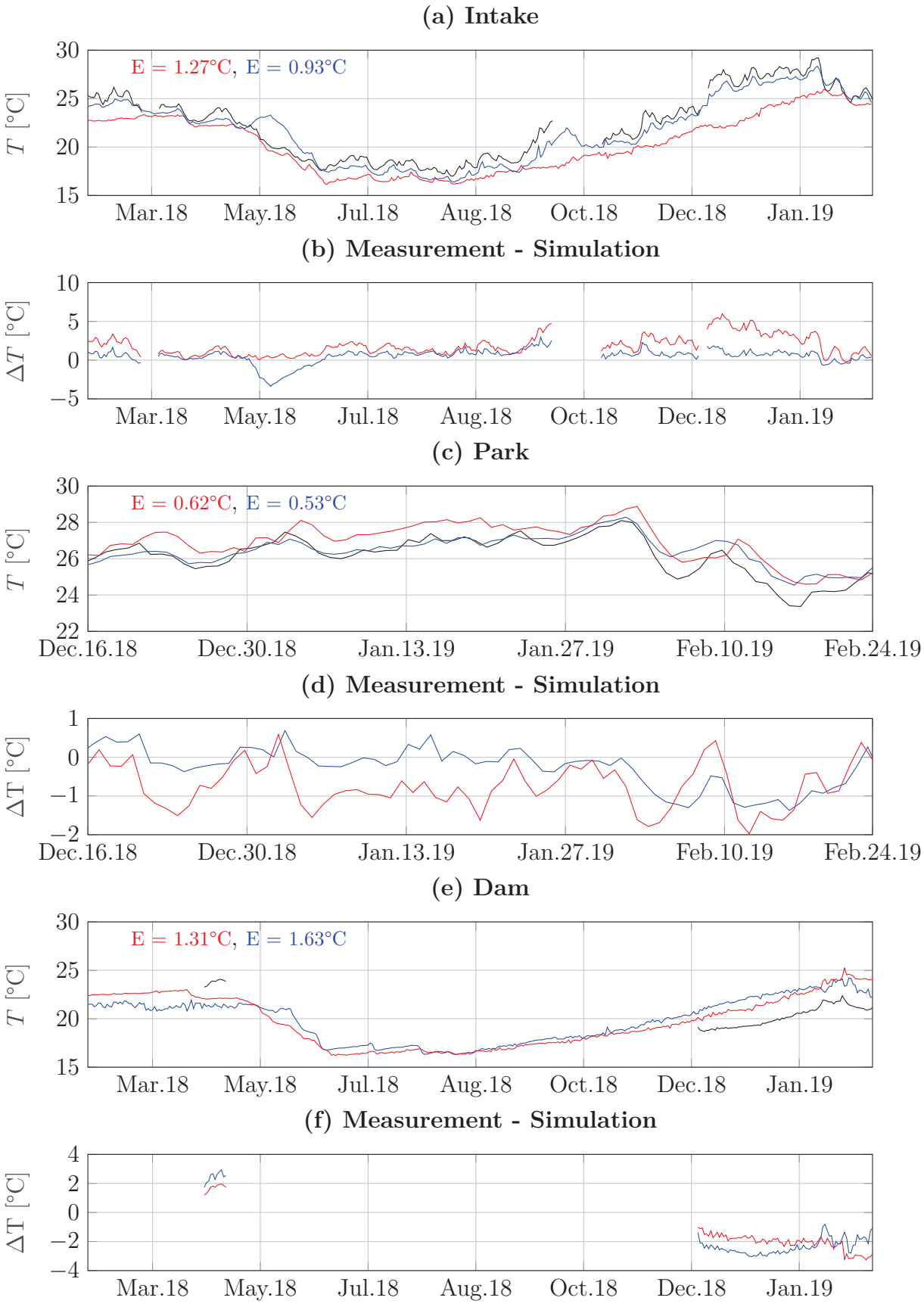


Figura 4.3: Comparison between measured by ABT and simulated water temperature for the Intake ((a) and (b)), Park ((c) and (d)) and Dam ((e) and (f)) observation points. Black lines represent the value measured by ABT, red lines the value simulated by Delft3D and blue lines represent the value simulated by CE-QUAL-W2.

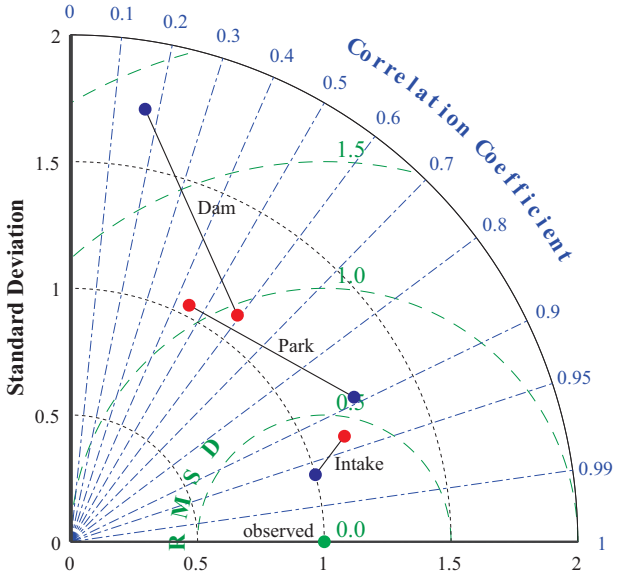


Figura 4.4: Taylor diagram for time series measured using ABTs and simulated using CE-QUAL-W2 (blue dots) and Delft3D (red dots) models.

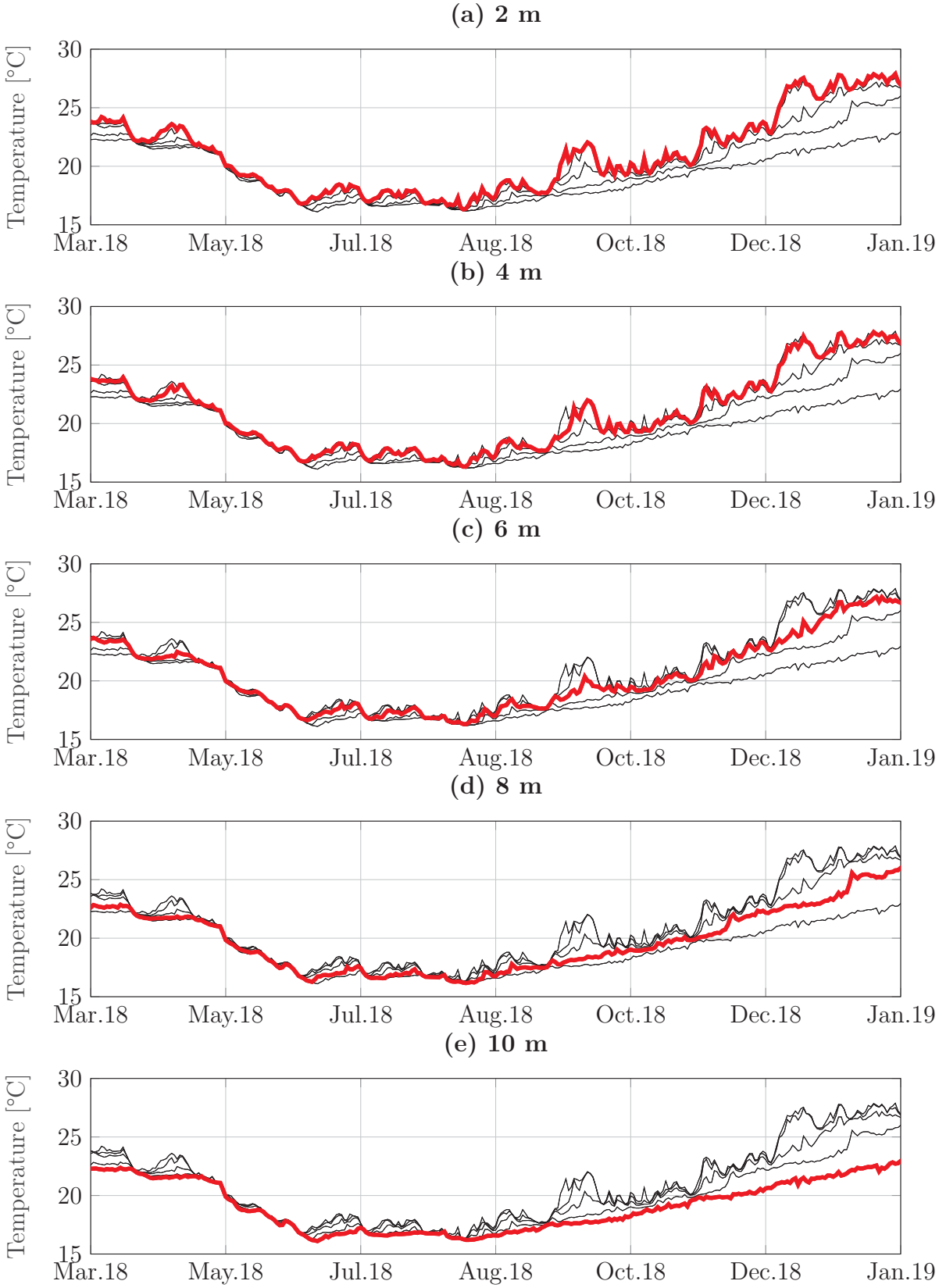


Figura 4.5: Time series measured by the thermistors chain at the intake region. Each sub-figure highlights only one depth.

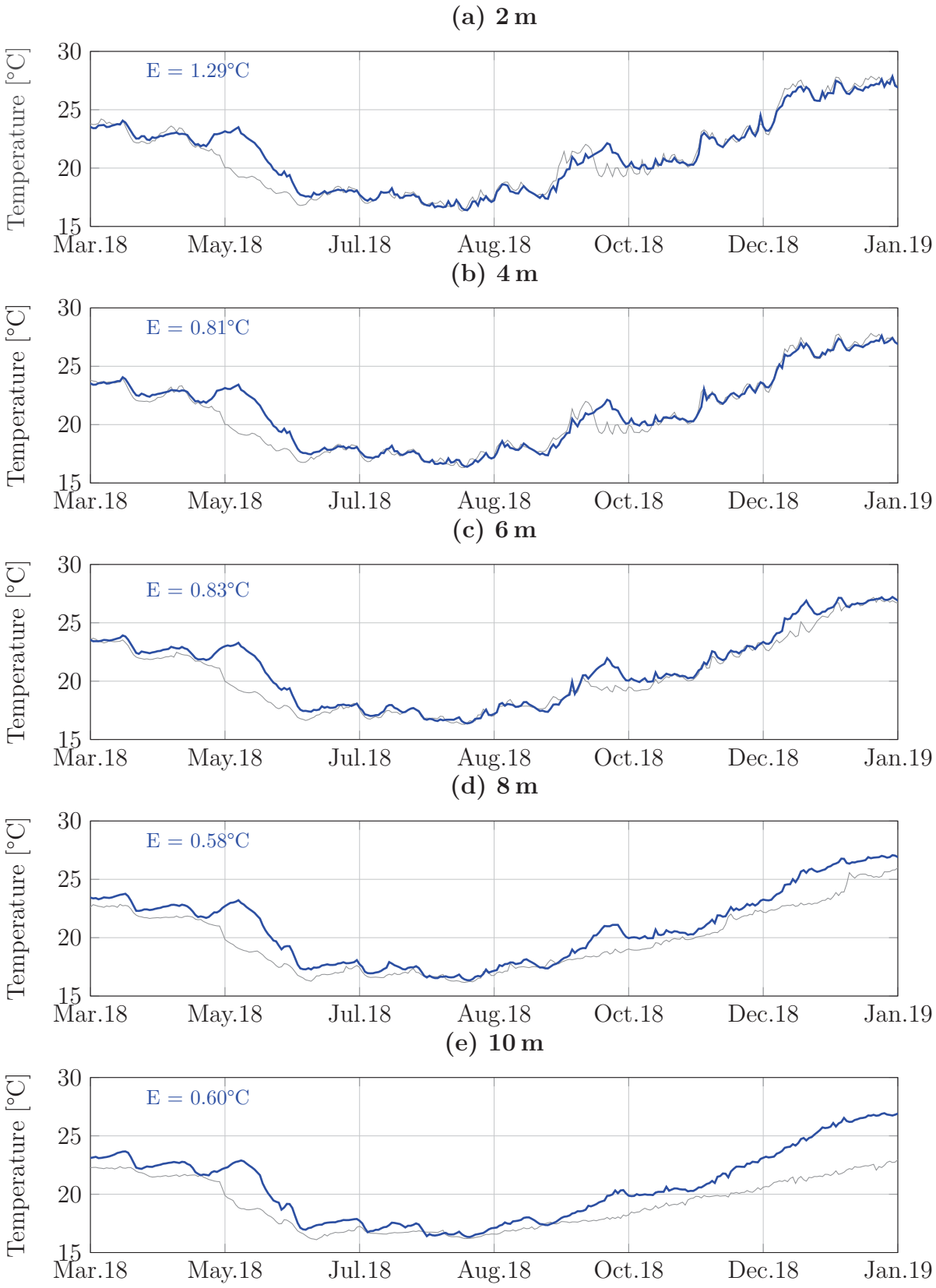


Figura 4.6: Time series measured by the thermistor chain (gray lines) and simulated by the CE-QUAL-W2 model (blue lines)

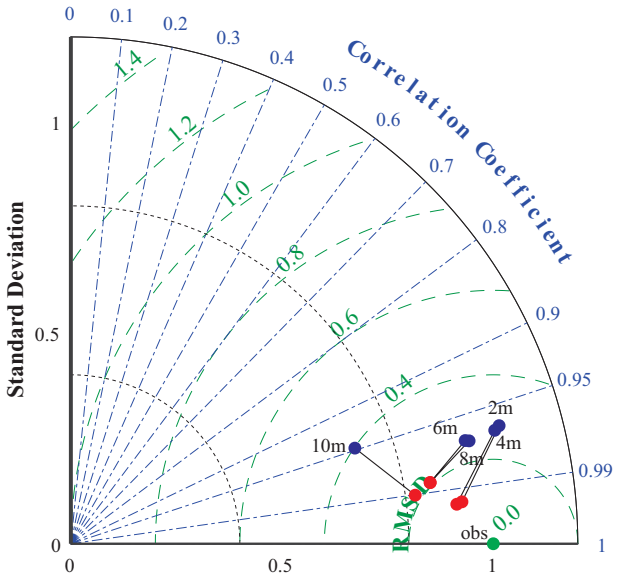


Figura 4.7: Taylor's diagram with the statistics of the models Delft3D (red) and CE-QUAL-W2 (blue) in comparison with the time series measured by the thermistors chains in the intake region.

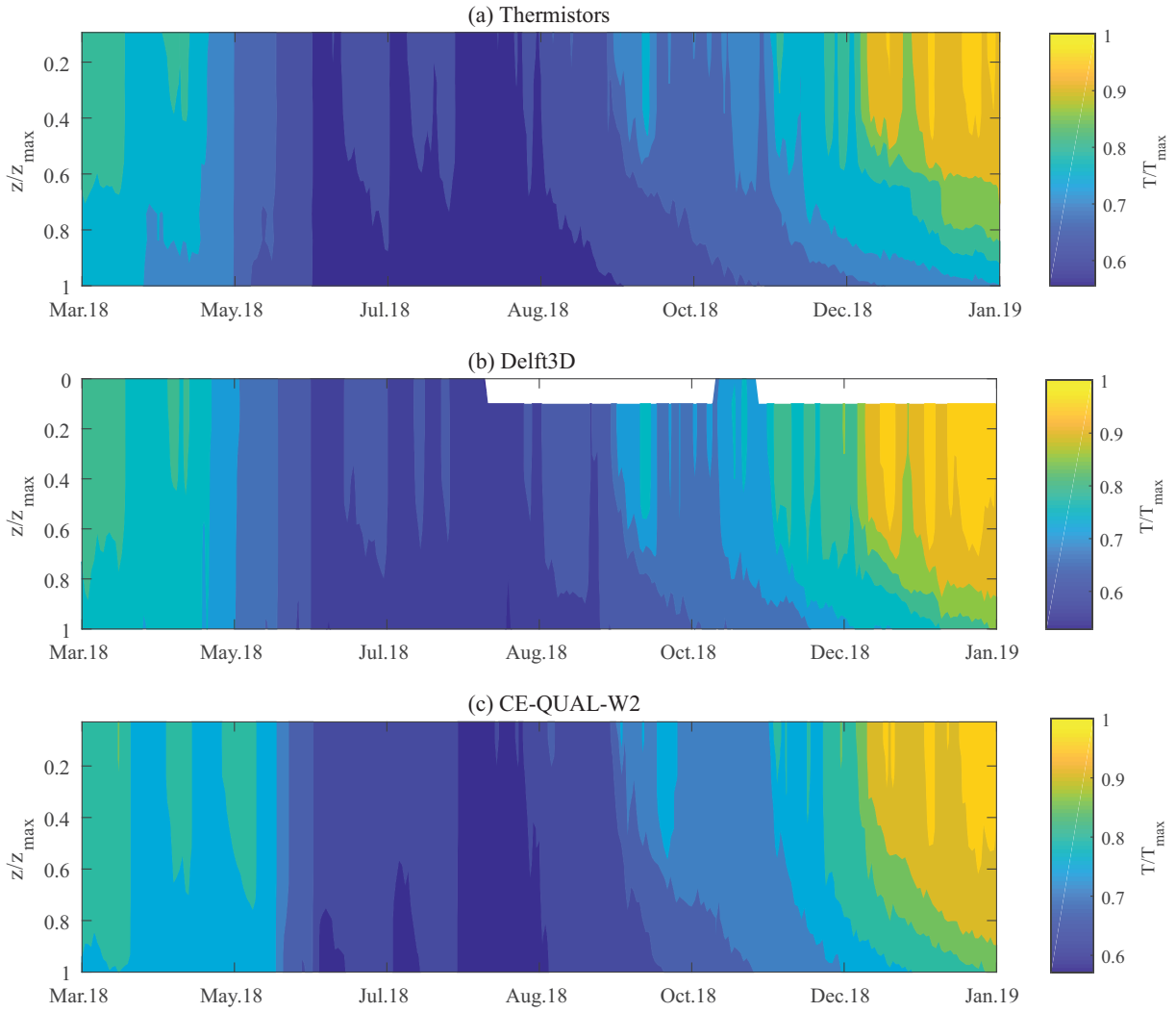


Figura 4.8: Contour plot of the evolution of the temperature profile at the intake. The white strips in the (b) Delft3D plot indicates a fluctuation in the water level.

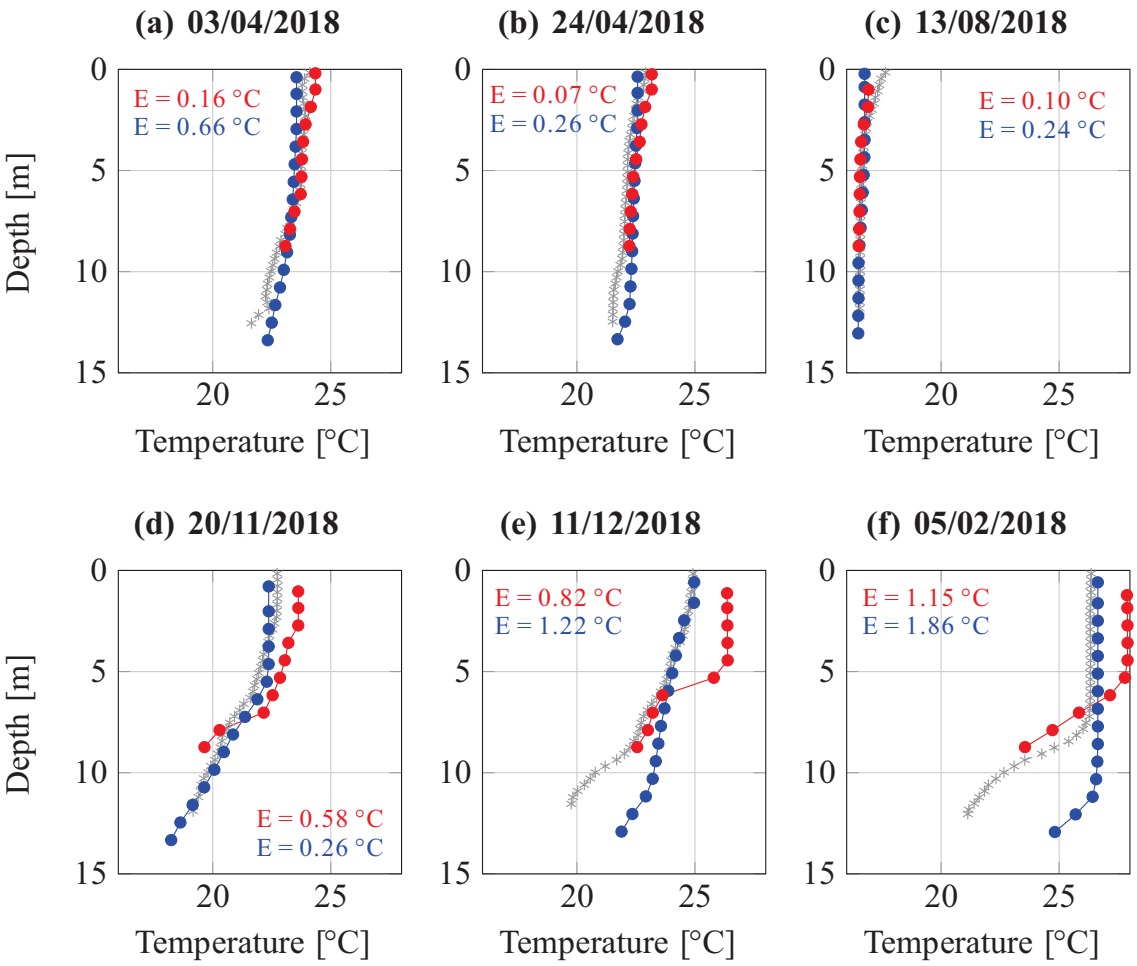


Figura 4.9: Profile of temperature at the Platform — Sanepar Intake. Temperature profiles measured by CTDs and simulated by the models. Gray lines represent the measurement, blue lines the simulated water temperature by CE-QUAL-W2 and red lines the simulated water temperature by Delft3D.

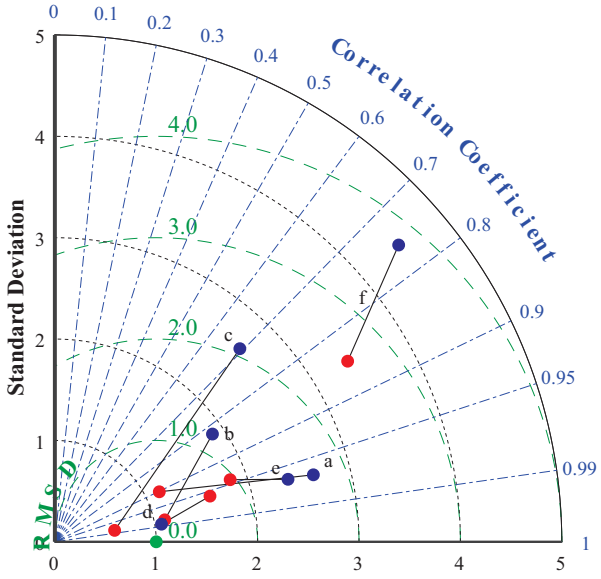


Figura 4.10: Taylor diagram with statistcs of the models Delft3D (red dots) and CE-QUAl-W2 (blue dots) in comparison with measured values. Statistics of the temperature profiles; see Figure 4.9 for the profiles.

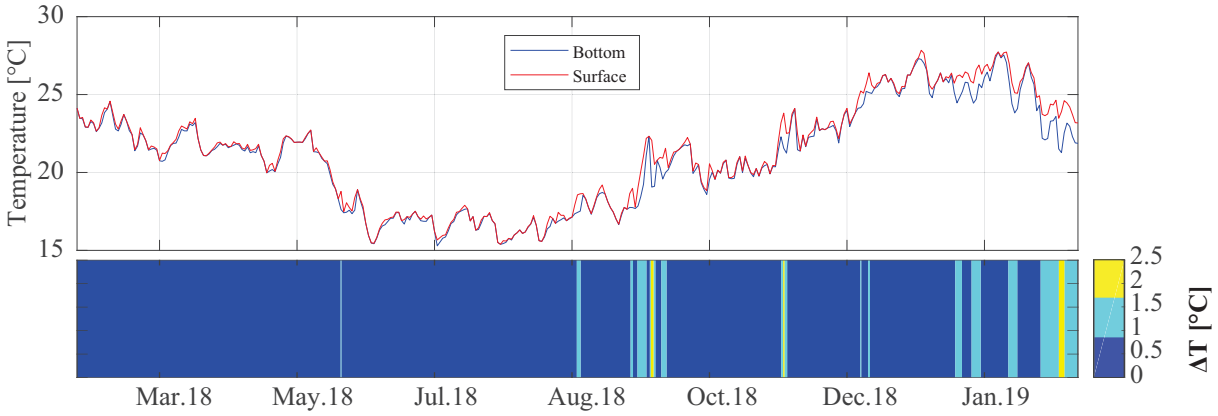


(a) Bridge

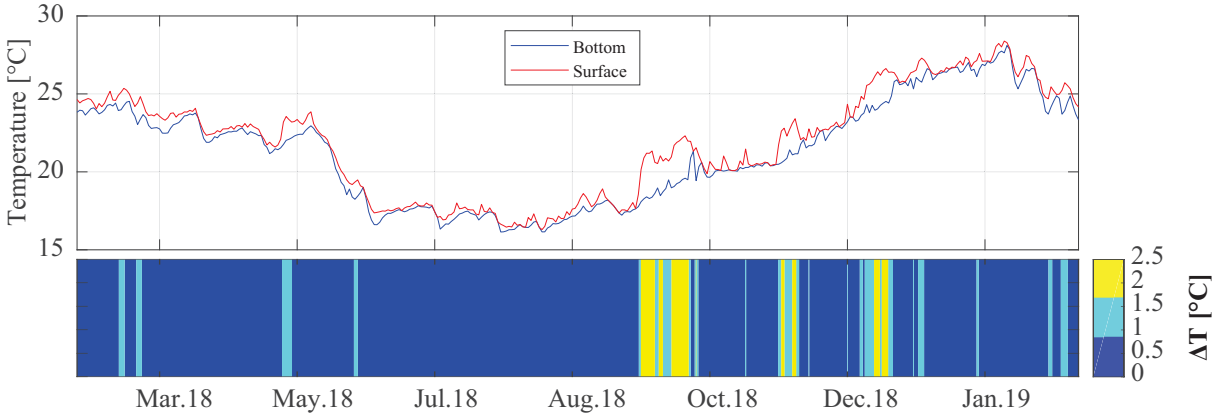


(b) Park

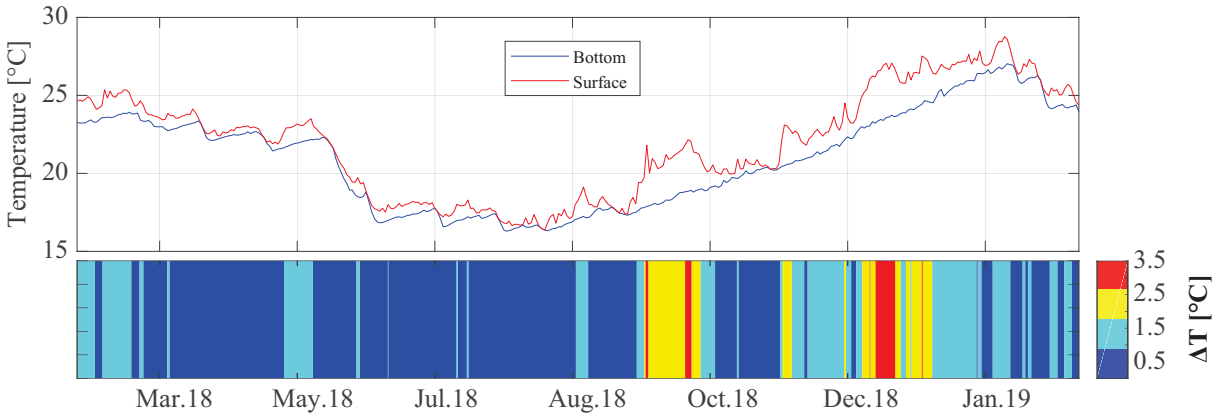


(c) Intake

Figura 4.11: Time series of temperature simulated by CE-QUAL-W2. In every subfigure the red line represents the temperature at the water level blue line the temperature at the bottom of the reservoir. The countourplot below each graph shows the diference between the two time series.

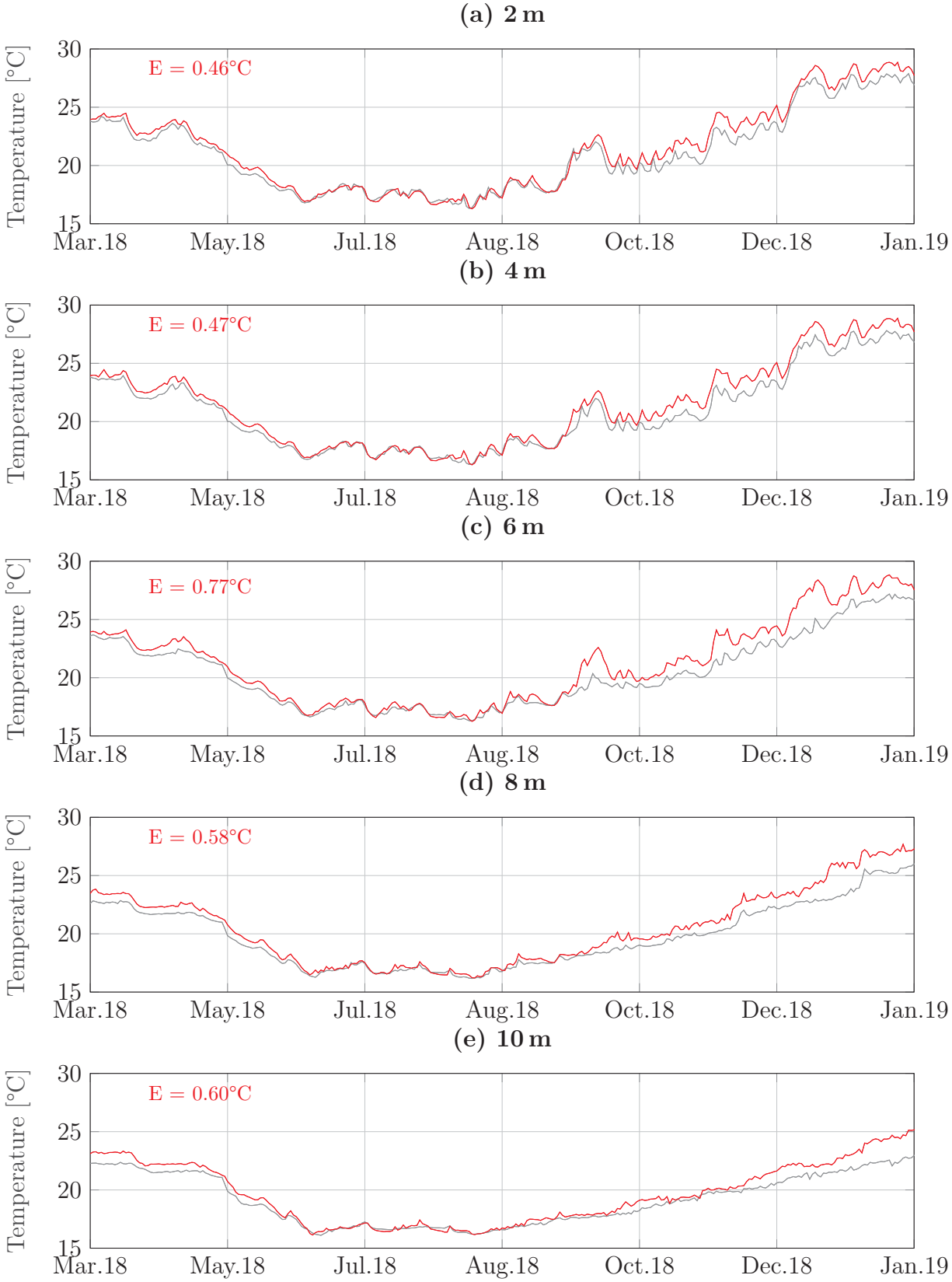


Figura 4.12: Time series measured by the thermistors chain (gray lines) and modeled by the Delft3D model (red lines).

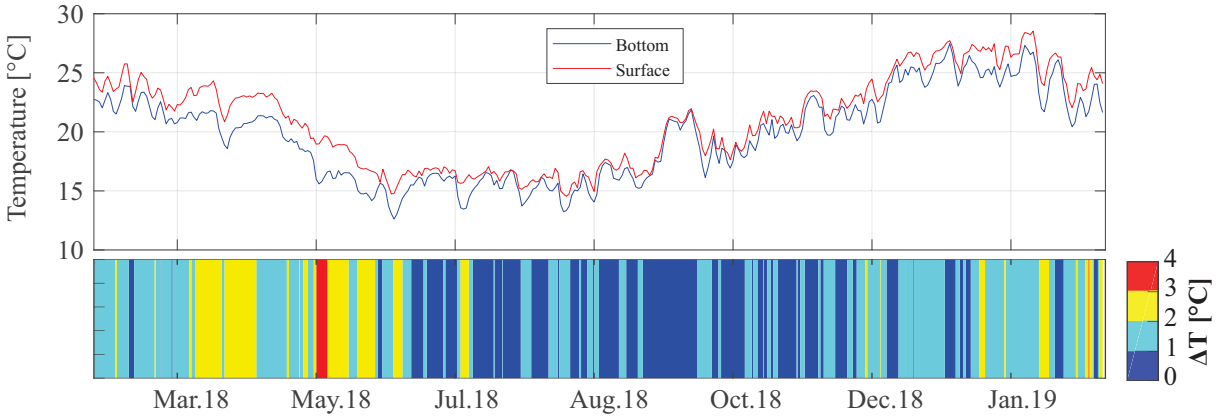


(a) Bridge

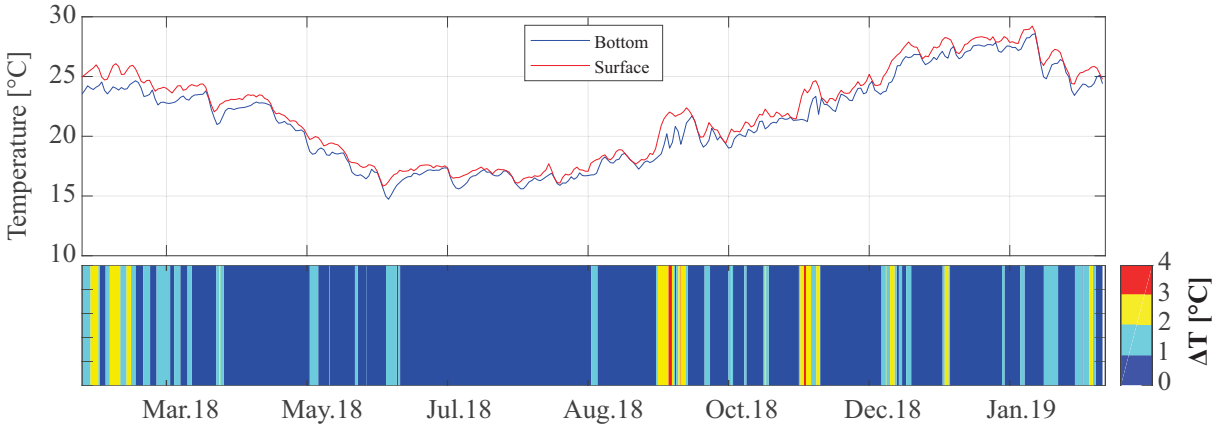


(b) Park

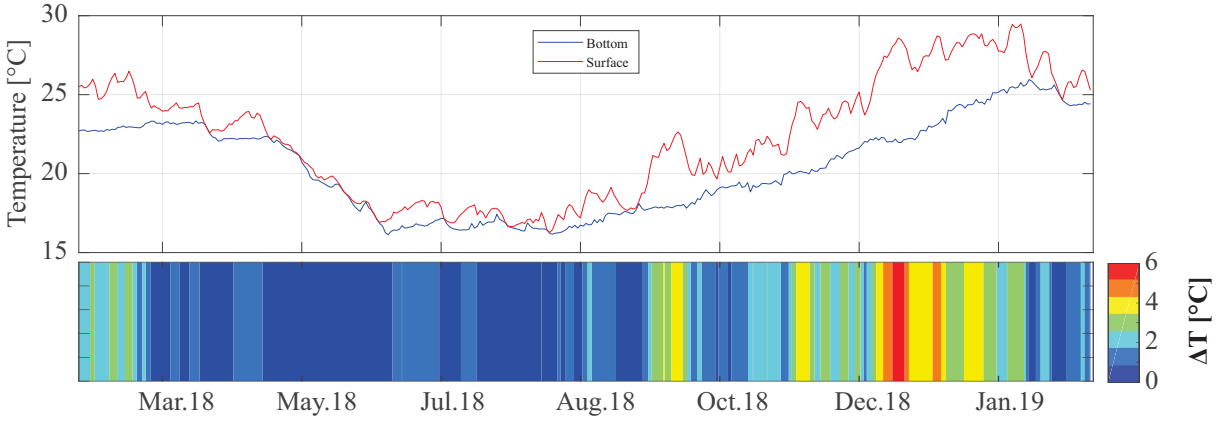


(c) Intake

Figura 4.13: Time series of temperature simulated by Delft3D. In every subfigure the red line represents the temperature at the water level blue line the temperature at the bottom of the reservoir. The countourplot below each graph shows the diference between the two time series.

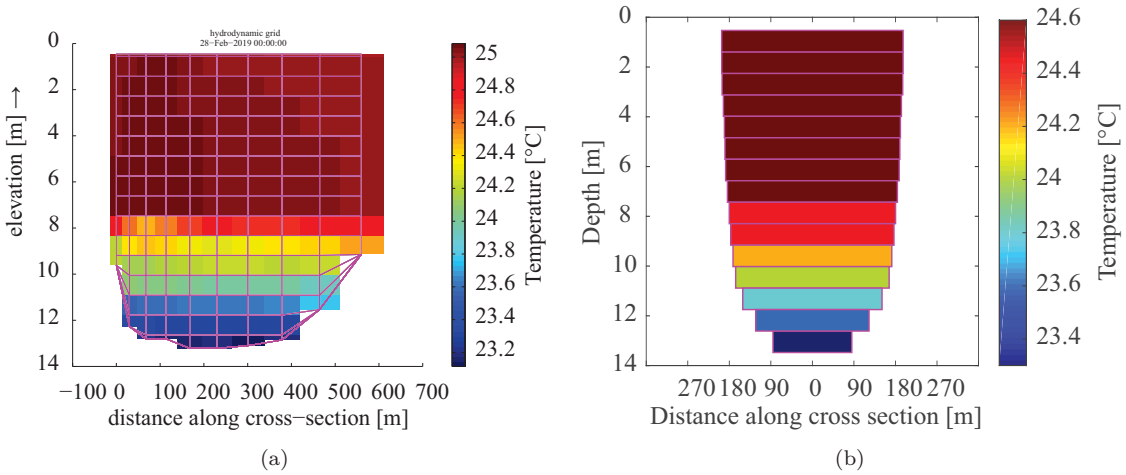


Figura 4.14: Transversal cross-section of the reservoir in (a) Delft3D and (b) in CE-QUAL-W2 for the intake region. The contour plot is for the last day of the simulation. In pink it is also shown the computational grid of both models.

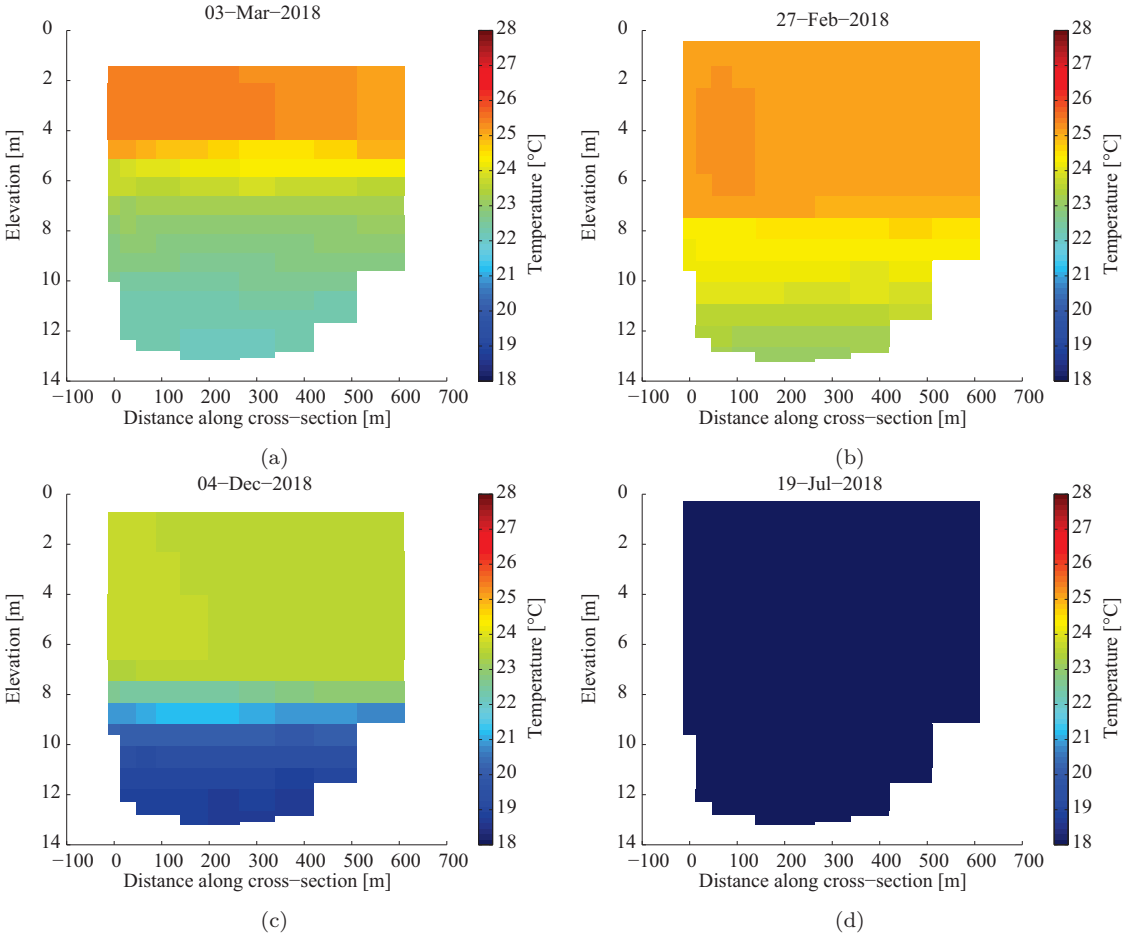


Figura 4.15: Transversal cross-section of the reservoir in Delft3D for the intake region at various dates depicting no strong variations in the transversal direction.

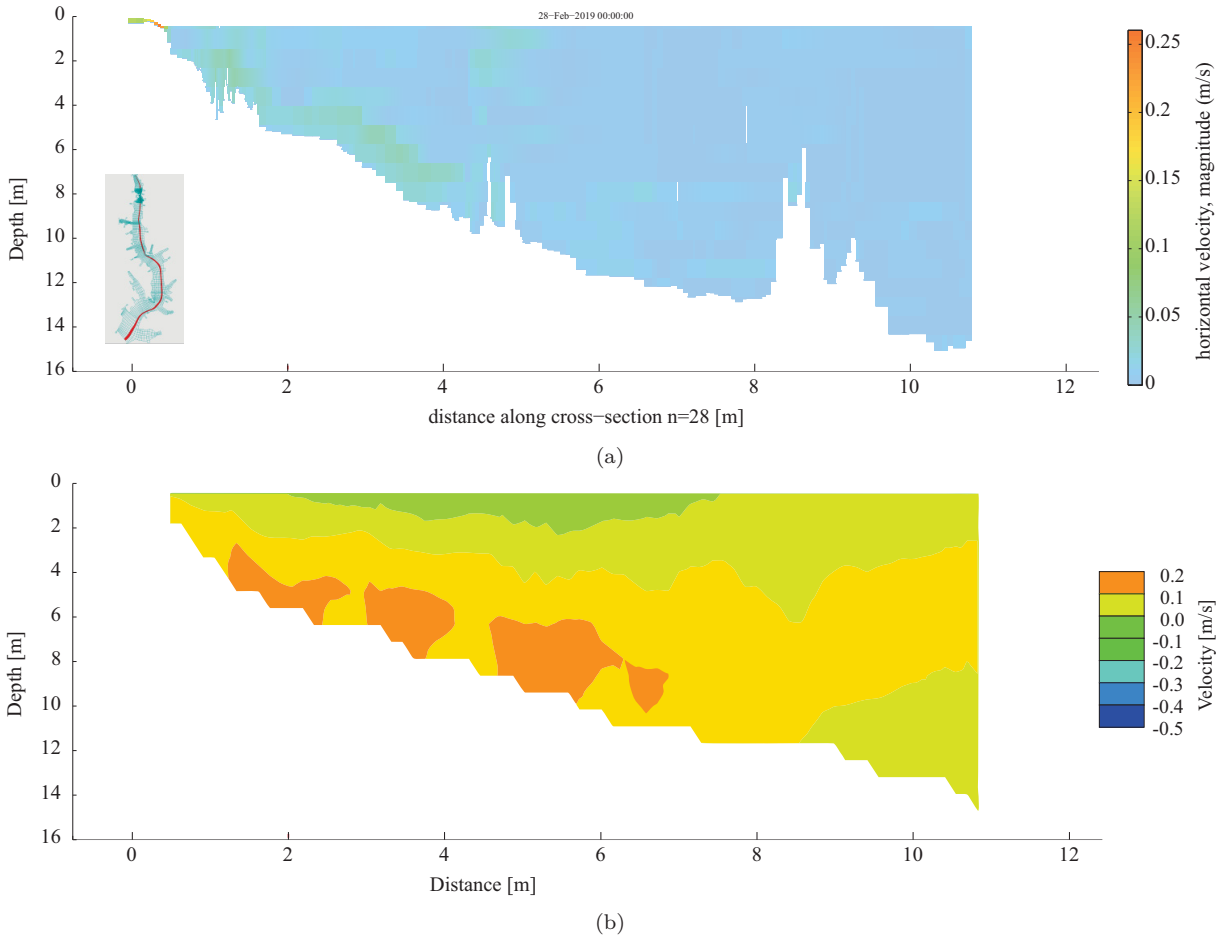


Figura 4.16: Longitudinal cross-section of the reservoir in (a) Delft3D and (b) in CE-QUAL-W2 showing the isolines of velocity. The contour plot is for the last day of the simulation.

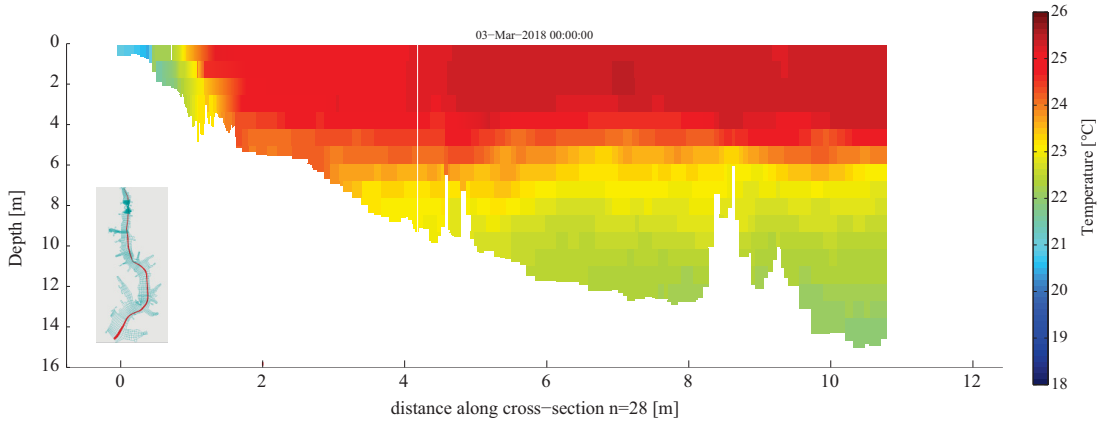


(a) Delft3D results.

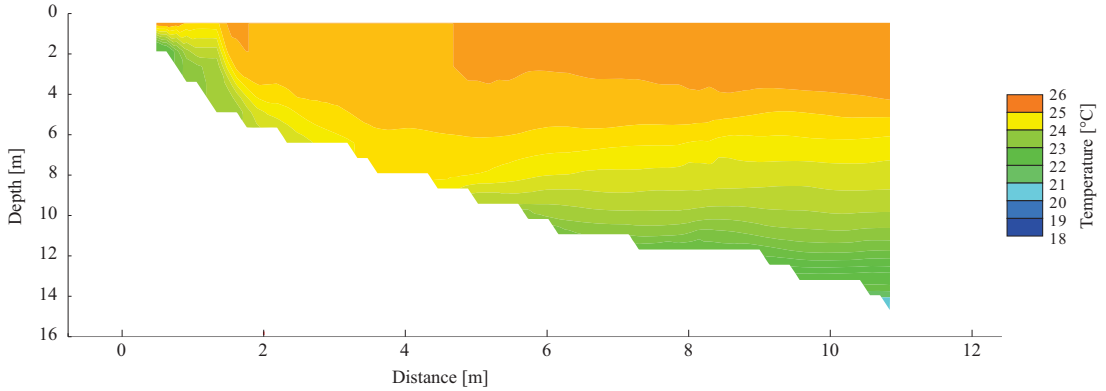


(b) CE-QUAL-W2 results.

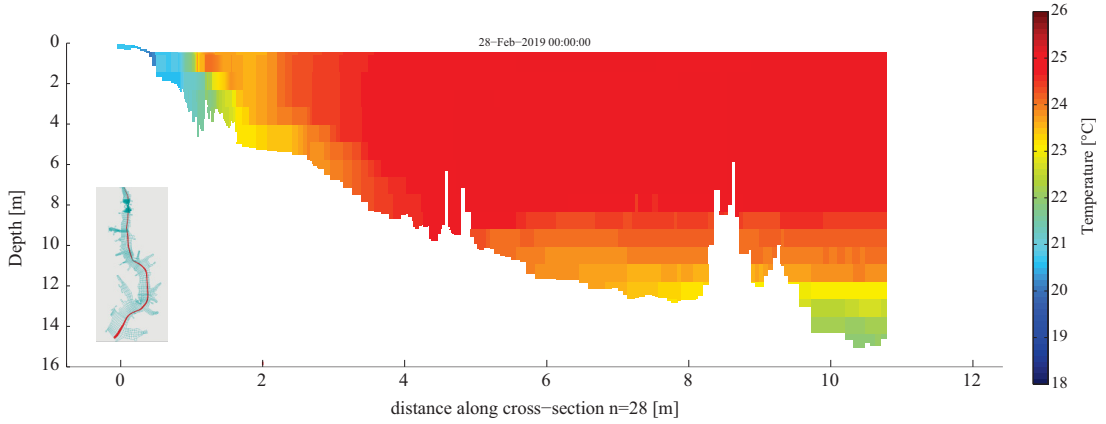


(c) Delft3D results.

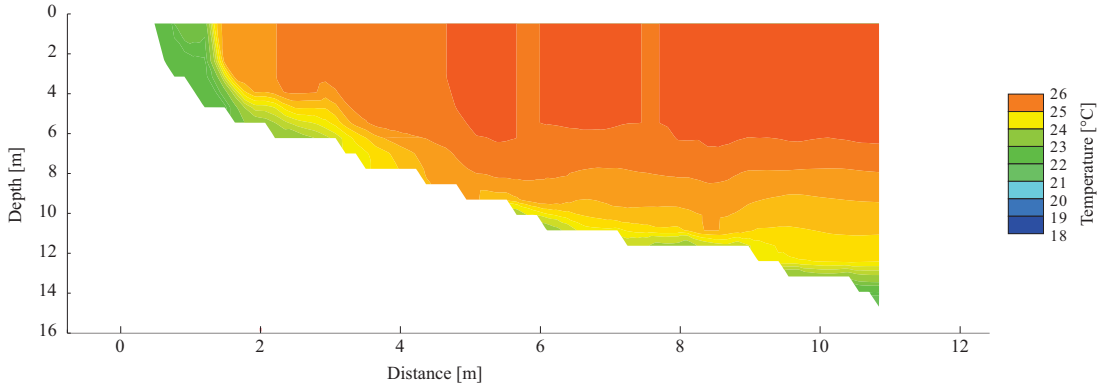


(d) CE-QUAL-W2 results.

Figura 4.17: Longitudinal cross-section of the reservoir in Delft3D and CE-QUAL-W2 showing isolines of temperature. (a) and (b) shows a interflow situation. (c) and (d) shows a underflow situation.

# 5 CONCLUSION

This study shows the capabilities of two models to assess the same problem. Both models used in this study were able to correctly predict the periods when the reservoir is mixed. Naturally, they can be used to predict the distribution of densities and concentrations of other substances by coupling models, as well as other important parameters for water quality and reservoir management.

Although using mean values for transversal variations, the two-dimensional models are capable of producing great results for reservoir simulations. Despite the limitations found in its construction and data treatment, the CE-QUAL-W2 model was able to produce results with a certain degree of parity with those generated by the 3D model. This model also has a wide range of water quality constituent transport models and it is thus highly recommended for studies using these materials.

Although the two-dimensional model has produced slightly worse results for the thermal stratification data, these results can be improved with efforts to calibrate their coefficients. When analyzing the time needed to run the simulation, the tradeoff is worthwhile. Even though three-dimensional models can produce exceptional results, the computational cost and complexity are very high and often prohibitive in its calibration and validation. However, once these results are generated and checked, they can be used in the confidence that they are currently the best options available.

As shown, the three-dimensional model did not show significant transversal variations for the intake region of the Passaúna reservoir. This type of analysis allowed a better understanding of the mechanisms that change the dynamics of the reservoir: If thermal stratification is the most relevant factor to be studied, 3D modeling is not necessary. The 2D model has been able to simulate temperature variations and incorporates hydrodynamic results.

As for hydrodynamics, the two-dimensional model showed slightly better results than the three-dimensional model. Although the velocities are always very low, the ability of the two-dimensional model to perceive variations in wind direction and speed is something noteworthy, since they are the main hydrodynamic forces in the reservoir.

In general, both models produced excellent quality results for the temperature and hydrodynamics of the studied water body. This fact along with the capabilities of the models to simulate almost any scenario puts them in a position of great importance in the area of water resources. However, in order to obtain reliable results, it is essential to provide the models with reliable data, thus having a management system committed to the acquisition, conference, and quality of measurements that serve as input for the models is necessary.

# REFERENCES


Afshar, A., Kazemi, H., and Saadatpour, M. (2011). Particle swarm optimization for automatic calibration of large scale water quality model (ce-qual-w2): Application to karkheh reservoir, iran. *Water resources management*, 25(10):2613–2632.

Angamuthu, B., Darby, S. E., and Nicholls, R. J. (2018). Impacts of natural and human drivers on the multi-decadal morphological evolution of tidally-influenced deltas. *Proceedings of the Royal Society A: Mathematical, Physical and Engineering Sciences*, 474(2219):20180396.

Barros, R. P. d. (2019). Aplicação do ce-qual-w2 para a modelagem da estrutura térmica do reservatório do descoberto df/go.

Bonnet, M.-P., Poulin, M., and Devaux, J. (2000). Numerical modeling of thermal stratification in a lake reservoir. methodology and case study. *Aquatic Sciences*, 62:105–124.

Cole, T. M. and Buchak, E. M. (1995). Ce-qual-w2: A two-dimensional, laterally averaged, hydrodynamic and water quality model, version 2.0. user manual. Technical report, ARMY ENGINEER WATERWAYS EXPERIMENT STATION VICKSBURG MS ENVIRONMENTAL LAB.

Conterato, T. M. et al. (2016). Simulação da qualidade da água do reservatório do vacacaí mirim utilizando o modelo ce-qual-w2.

Cox, J. N. (2010). Advantages and practicality of using a 2d hydrodynamicmodel in comparison to a 1d hydrodynamic model in aflood prone area. Master's thesis, University of Southern Queensland, Queensland.

de Farias Mesquita, J. B., Neto, I. E. L., Raabe, A., and de Araújo, J. C. (2020). The influence of hydroclimatic conditions and water quality on evaporation rates of a tropical lake. *Journal of Hydrology*, 590:125456.

Deltares (2014). User manual Delft3D-Flow. Technical report, Deltares, Delft, The Netherlands.

Dutta, R. K. and Das, B. (2020). Modeling curtain weirs for controlling algal blooms in the largest tributary of the three gorges reservoir, china. *Alexandria Engineering Journal*.

Falkenberg, A. V. (2009). *Estudo da dispersão, mistura e qualidade da água do Complexo Estuarino de Paranaguá com uso de modelagem numérica*. PhD thesis, Dissertation, Universidade Federal do Paraná.

Ferreira, J. P. M. (2019). *Avaliação da dispersão das plumas dos emissários submarinos no canal de São Sebastião (estado de São Paulo, Brasil), através da modelagem numérica.* PhD thesis, Universidade de São Paulo.

Fischer, H., List, J., Koh, C., Imberger, J., and Brooks, N. (2013). *Mixing in Inland and Coastal Waters*. Elsevier Science.

Gastaldini, M. d. C. C., PAZ, M., KRAEMER, M., PAIVA, E., and PAIVA, J. (2004). Aplicação de modelo matemático a dados de ciclos de estratificação térmica e de qualidade da água do reservatório do vacacaí-mirim. *Revista Brasileira de Recursos Hídricos, Porto Alegre*, 9(1):27–35.

Gerritsen, H., Goede, E., Platzek, F., Kester, J., Genseberger, M., and Uittenbogaard, R. (2008). Validation document delft3d-flow; a software system for 3d flow simulations.

He, W., Lian, J., Yao, Y., Wu, M., and Ma, C. (2017). Modeling the effect of temperature-control curtain on the thermal structure in a deep stratified reservoir. *Journal of Environmental Management*, 202:106–116.

Hipsey, M. R., Bruce, L. C., Boon, C., Busch, B., Carey, C. C., Hamilton, D. P., Hanson, P. C., Read, J. S., de Sousa, E., Weber, M., and Winslow, L. A. (2019). A general lake model (glm 3.0) for linking with high-frequency sensor data from the global lake ecological observatory network (gleon). *Geoscientific Model Development*, 12(1):473–523.

Ji, Z. (2008). *Hydrodynamics and Water Quality*. John Wiley & sons, inc.

Kaçıkoç, M. and Beyhan, M. (2014). Hydrodynamic and water quality modeling of lake eğirdir. *CLEAN – Soil, Air, Water*, 42(11):1573–1582.

Kasvi, E., Alho, P., Lotsari, E., Wang, Y., Kukko, A., Hyyppä, H., and Hyyppä, J. (2015). Two-dimensional and three-dimensional computational models in hydrodynamic and morphodynamic reconstructions of a river bend: sensitivity and functionality. *Hydrological Processes*, 29(6):1604–1629.

Kurup, R. G., Hamilton, D. P., and Phillips, R. L. (2000). Comparison of two 2-dimensional, laterally averaged hydrodynamic model applications to the swan river estuary. *Mathematics and Computers in Simulation*, 51(6):627 – 638.

Lane, R. (2019). Lake. Encyclopædia Britannica, inc. `https://www.britannica.com/science/lake/`. Access Date: 21/06/2019.

Leonard, B. P. (1979). A stable and accurate convective modelling procedure based on quadratic upstream interpolation. *Computer methods in applied mechanics and engineering*, 19(1):59–98.

Lindenschmidt, K. (2006). The effect of complexity on parameter sensitivity and model uncertainty in river water quality modelling. *Ecological Modeling*, 109.

Lindenschmidt, K.-E., Carr, M. K., Sadeghian, A., and Morales-Marin, L. (2019). CE-QUAL-W2 model of dam outflow elevation impact on temperature, dissolved oxygen and nutrients in a reservoir. *Scientific Data*, 6(1):1–7.

Martin, J. and McCutcheon, S. (2018). *Hydrodynamics and Transport for Water Quality Modeling*. CRC Press.

Nascimento, V. V. d. (2019). Uso do modelo delft3d no estudo da dispersão de propágulos de mangue no estuário do rio pacoti.

Niño, Y. and Tamburrino, A. (2004). Heat balance in lakes and reservoirs. `https://www.u-cursos.cl/ingenieria/2005/1/CI71Q/1/material_docente/bajar?id_material=29468`. Access Date: 08/07/2019.

Ostfeld, A. and Salomons, S. (2005). A hybrid genetic - instance based learning algorithm for ce-qual-w2 calibration. *Journal of Hydrology - J HYDROL*, 310.

Pereira, R. d. S. (2003). Processo que regem a qualidade da água da lagoa dos patos, segundo o modelo delft3d. Master's thesis.

Pion, S. M. (2018). *Modelagem computacional de qualidade da água aplicada a reservatório de abastecimento público da região metropolitana de São Paulo.* PhD thesis, Universidade de São Paulo.

Poletto, F. M. (2013). Determinação das possíveis áreas de risco atingidas por um derrame hipotético de óleo na área de fundeio do porto de itajaí-sc utilizando o modelo numérico delft3d.

Polli, B. A. (2014). Modelagem 1D do fluxo vertical de calor em corpos de água horizontalmente homogêneos. Masters dissertation. Master's thesis, Pós-Graduação em Engenharia de Recursos Hídricos e Ambiental - Universidade Federal do Paraná, Curitiba - PR.

Polli, B. A. (2018). *Modeling of heat transport in lakes: spatial and temporal characterization.* PhD thesis, Pós-Graduação em Engenharia de Recursos Hídricos e Ambiental - Universidade Federal do Paraná, Curitiba - PR. 149 pgs.

Portland, S. U. (2019). Application by country – CE-QUAL-W2. `http://www.cee.pdx.edu/w2/`. Access Date: 12/08/2019.

Sabeti, R., Jamali, S., and Jamali, H. H. (2017). Simulation of thermal stratification and salinity using the ce-qual-w2 model (case study: mamloo dam). *Engineering, Technology & Applied Science Research*, 7(3):1664–1669.

SisBaHiA (2019). Referência técnica do SisBaHiA. Technical report, COPPE/UFRJ, Rio de Janeiro RJ.

Socolofsky, S. A. and Jirka, G. H. (2005). *Special Topics in Mixing and Transport Processes in the Environment.* Coastal and Ocean Engineering Division. Texas A&M University.

Sousa, M. M. (2010). ComparaÇÃo entre ferramentas de modelagem unidimensional e quasi-bidimensional, permanente e nÃo-permanente, em planejamento e projetos de engenharia hidrÁulica. Master's thesis, COPPE — Universidade Federal do Rio de Janeiro, Rio de Janeiro.

Taylor, K. E. (2001). Summarizing multiple aspects of model performance in a single diagram. *Journal of Geophysical Research: Atmospheres*, 106(D7):7183–7192.

Theol, S. A., Jagers, B., Suryadi, F., and de Fraiture, C. (2019). The use of delft3d for irrigation systems simulations. *Irrigation and Drainage*, 68(2):318–331.

Tomas, G. P. (2014). Avaliação hidromorfológica do uso de espigões em hidrovias.

Torres, E., Galván, L., Cánovas, C. R., Soria-Píriz, S., Arbat-Bofill, M., Nardi, A., Papaspyrou, S., and Ayora, C. (2016). Oxycline formation induced by fe (ii) oxidation in a water reservoir affected by acid mine drainage modeled using a 2d hydrodynamic and water quality model—ce-qual-w2. *Science of the Total Environment*, 562:1–12.

UNESCO (1981). Background papers and supporting data on the international equation of state 1980. Technical report, UNESCO, Paris, France.

Versteeg, H. K. and Malalasekera, W. (2007). *An Introduction to Computational Fluid Dynamics*. Pearson Education Limited.

Villaret, C., Hervouet, J.-M., Kopmann, R., Merkel, U., and Davies, A. (2013). Morphodynamic modeling using the telemac finite-element system. *Computers and Geosciences - COMPUT GEOSCI*, 53.

Yang, S. H. and Harari, J. (2016). Modeling extreme conditions of sewage plumes in central-south coastal region of são paulo state-brazil. *Revista DAE*, (204):73–80.

Yang, Y., Yun, D., Tuo, Y., and He, T. (2019). Influence of temperature control curtain on water temperature structure and flow pattern in reservoir. *E-proceedings of the 38th IAHR World Congress*, 6(1):1–11.